Pharmacological Research 152 (2020) 104609

Contents lists available at ScienceDirect

Pharmacological Research

journal homepage: www.elsevier.com/locate/yphrs

Invited Review

Properties of FDA-approved small molecule protein kinase inhibitors: A 2020 update

Robert Roskoski Jr.

Blue Ridge Institute for Medical Research, 3754 Brevard Road, Suite 116, Box 19, Horse Shoe, North Carolina, 28742-8814, United States

ARTICLE INFO

Chemical compounds studied in this article:
Binimetinib (PubMED CID: 10288191)
Crizotinib (PubMED CID: 9033117)
Dabrafenib (PubMED CID: 44462760)
Entrectinib (PubMED CID: 25141092)
Erdafitinib (PubMED CID: 67462786)
Fedratinib (PubMED CID: 16722836)
Imatinib (PubMED CID: 123596)
Pexidartinib (PubMED CID: 25151352)
Sorafenib (PubMED CID: 216239)
Trametinib (PubMED CID: 11707110)

Keywords:
Catalytic spine
Hydrophobic interaction
Protein kinase inhibitor classification
Protein kinase structure
Regulatory spine
Shell residues

ABSTRACT

Because genetic alterations including mutations, overexpression, translocations, and dysregulation of protein kinases are involved in the pathogenesis of many illnesses, this enzyme family is currently the subject of many drug discovery programs in the pharmaceutical industry. The US FDA approved four small molecule protein kinase antagonists in 2019; these include entrectinib, erdafitinib, pexidartinib, and fedratinib. Entrectinib binds to TRKA/B/C and ROS1 and is prescribed for the treatment of solid tumors with NTRK fusion proteins and for ROS1-postive non-small cell lung cancers. Erdafitinib inhibits fibroblast growth factor receptors 1–4 and is used in the treatment of urothelial bladder cancers. Pexidartinib is a CSF1R antagonist that is prescribed for the treatment of tenosynovial giant cell tumors. Fedratinib blocks JAK2 and is used in the treatment of myelofibrosis. Overall, the US FDA has approved 52 small molecule protein kinase inhibitors, nearly all of which are orally effective with the exceptions of temsirolimus (which is given intravenously) and netarsudil (an eye drop). Of the 52 approved drugs, eleven inhibit protein-serine/threonine protein kinases, two are directed against dual specificity protein kinases, eleven target non-receptor protein-tyrosine kinases, and 28 block receptor protein-tyrosine kinases. The data indicate that 46 of these drugs are used in the treatment of neoplastic diseases (eight against non-solid tumors such as leukemias and 41 against solid tumors including breast and lung cancers; some drugs are used against both tumor types). Eight drugs are employed in the treatment of non-malignancies: fedratinib, myelofibrosis; ruxolitinib, myelofibrosis and polycythemia vera; fostamatinib, chronic immune thrombocytopenia; baricitinib, rheumatoid arthritis; sirolimus, renal graft vs. host disease; nintedanib, idiopathic pulmonary fibrosis; netarsudil, glaucoma; and tofacitinib, rheumatoid arthritis, Crohn disease, and ulcerative colitis. Moreover, sirolimus and ibrutinib are used for the treatment of both neoplastic and non-neoplastic diseases. Entrectinib and larotrectinib are tissue-agnostic anti-cancer small molecule protein kinase inhibitors. These drugs are prescribed for the treatment of any solid cancer harboring NTRK1/2/3 fusion proteins regardless of the organ, tissue, anatomical location, or histology type. Of the 52 approved drugs, seventeen are used in the treatment of more than one disease. Imatinib, for example, is approved for the treatment of eight disparate disorders. The most common drug targets of the approved pharmaceuticals include BCR-Abl, B-Raf, vascular endothelial growth factor receptors (VEGFR), epidermal growth factor receptors (EGFR), and ALK. Most of the approved small molecule protein kinase antagonists (49) bind to the protein kinase domain and six of them bind covalently. In contrast, everolimus, temsirolimus, and sirolimus are larger molecules (MW ≈ 1000) that bind to FK506 binding protein-12 (FKBP-12) to generate a complex that inhibits the mammalian target of rapamycin (mTOR) protein kinase complex. This review presents the physicochemical properties of all of the FDA-approved small molecule protein kinase inhibitors. Twenty-two of the 52 drugs have molecular weights greater than 500, exceeding a Lipinski rule of five criterion. Excluding the macrolides (everolimus, sirolimus, temsirolimus), the average molecular weight of the approved drugs is 480 with a range of 306 (ruxolitinib) to 615 (trametinib). More than half of the antagonists (29) have lipophilic efficiency values of less than five while the recommended optima range from 5 to 10. One of the troublesome problems with both targeted and cytotoxic

Abbreviations: ALL, acute lymphoblastic leukemia; AS, activation segment; BP, back pocket; C-spine, catalytic spine; CDK, cyclin-dependent protein kinase; CML, chronic myelogenous leukemia; CS1, catalytic spine residue 1; CL, catalytic loop; EGFR, epidermal growth factor receptor; F, front pocket; FGFR, fibroblast growth factor receptor; FKBP12/mTOR, FK Binding Protein-12/mammalian target of rapamycin; GK, gatekeeper; GRL, glycine-rich loop; KLIFS-3, kinase-ligand interaction fingerprint and structure residue-3; LE, ligand efficiency; LipE, lipophilic efficiency; NSCLC, non-small cell lung cancer; PDGFR, platelet-derived growth factor receptor; PI3K, phosphatidylinositol 3-kinase; PKA, protein kinase A; Ro5, Lipinski's rule of five; R-spine, regulatory spine; RS1, regulatory spine residue 1; Sh2, shell residue 2; VEGFR, vascular endothelial growth factor receptor

E-mail address: rrj@brimr.org.

https://doi.org/10.1016/j.phrs.2019.104609
Received 14 December 2019; Accepted 16 December 2019
Available online 17 December 2019

drugs in the treatment of malignant diseases is the near universal development of resistance to every therapeutic modality.

Table 1
FDA-approved small molecule protein kinase inhibitors, their protein kinase targets, and therapeutic indications.

Drug (Code) Trade name	Year approved	Primary targets[a]	Therapeutic indications[b]
Abemaciclib (LY2835219) Verzenio	2017	CDK4/6	Combination therapy with an (i) aromatase inhibitor or with (ii) fulvestrant or as a monotherapy for breast cancers
Acalabrutinib (ACP-196) Calquence	2017	BTK	Mantle cell lymphomas, CLL, SLL
Afatinib (BIBW 2992) Tovok	2013	ErbB1/2/4	NSCLC
Alectinib (CH5424802) Alecensa	2015	ALK, RET	ALK-positive NSCLC
Axitinib (AG-013736) Inlyta	2012	VEGFR1/2/3	RCC
Baricitinib (LY 3009104) Olumiant	2018	JAK1/2	Rheumatoid arthritis
Binimetinib (MEK162) Mektovi	2018	MEK1/2	Combination therapy with encorafenib for $BRAF^{V600E/K}$ melanomas
Bosutinib (SKI-606) Bosulif	2012	BCR-Abl	CML
Brigatinib (AP 26113) Alunbrig	2017	ALK	ALK-positive NSCLC
Cabozantinib (BMS-907351) Cometriq	2012	RET, VEGFR2	Medullary thyroid cancers, RCC, HCC
Ceritinib (LDK378) Zykadia	2014	ALK	ALK-positive NSCLC resistant to crizotinib
Cobimetinib (GDC-0973) Cotellic	2015	MEK1/2	$BRAF^{V600E/K}$ melanomas in combination with vemurafenib
Crizotinib (PF 2341066) Xalkori	2011	ALK, ROS1	ALK or ROS1-postive NSCLC
Dabrafenib (GSK2118436) Tafinlar	2013	B-Raf	$BRAF^{V600E/K}$ melanomas, $BRAF^{V600E}$ NSCLC, $BRAF^{V600E}$ anaplastic thyroid cancers
Dacomitinib (PF-00299804) Visimpro	2018	EGFR	*EGFR*-mutant NSCLC
Dasatinib (BMS-354825) Sprycell	2006	BCR-Abl	CML
Encorafenib (LGX818) Braftovi	2018	B-Raf	Combination therapy with binimetinib for $BRAF^{V600E/K}$ melanomas
Entrectinib (RXDX-101) Rozlytrek	2019	TRKA/B/C, ROS1	Solid tumors with NTRK fusion proteins, ROS1-positive NSCLC
Erdafitinib (JNJ-42756493) Balversa	2019	FGFR1/2/3/4	Urothelial bladder cancers
Erlotinib (OSI-774) Tarceva	2004	EGFR	NSCLC, pancreatic cancers
Everolimus (RAD001) Afinitor	2009	FKBP12/mTOR	HER2-negative breast cancers, pancreatic neuroendocrine tumors, RCC, angiomyolipomas, subependymal giant cell astrocytomas
Fedratinib (TG101348) Inrebic	2019	JAK2	Myelofibrosis
Fostamatinib (R788) Tavalisse	2018	Syk	Chronic immune thrombocytopenia
Gefitinib (ZD1839) Iressa	2003	EGFR	NSCLC
Gilteritinib (ASP2215) Xospata	2018	Flt3	AML
Ibrutinib (PCI-32765) Imbruvica	2013	BTK	CLL, mantle cell lymphomas, marginal zone lymphomas, graft vs. host disease
Imatinib (STI571) Gleevec	2001	BCR-Abl	Ph^+ CML or ALL, aggressive systemic mastocytosis, chronic eosinophilic leukemias, dermatofibrosarcoma protuberans, hypereosinophilic syndrome, GIST, myelodysplastic/myeloproliferative disease
Lapatinib (GW572016) Tykerb	2007	EGFR, ErbB2/HER2	HER2-positive breast cancers
Larotrectinib (LOXO-101) Vitrakvi	2018	TRKA/B/C	Solid tumors with NTRK fusion proteins
Lenvatinib (AK175809) Lenvima	2015	VEGFR, RET	Differentiated thyroid cancers
Lorlatinib (PF-06463922) Lorbrena	2018	ALK	ALK-positive NSCLC
Midostaurin (CPG 41251) Rydapt	2017	Flt3	AML, mastocytosis, mast cell leukemias
Neratinib (HKI-272) Nerlynx	2017	ErbB2/HER2	HER2-positive breast cancers
Netarsudil (AR11324) Rhopressa	2018	ROCK1/2	Glaucoma
Nilotinib (AMN107) Tasigna	2007	BCR-Abl	Ph^+ CML
Nintedanib (BIBF-1120) Vargatef	2014	FGFR1/2/3	Idiopathic pulmonary fibrosis
Osimertinib (AZD-9292) Tagrisso	2015	*EGFR* T970M	NSCLC
Palbociclib (PD-0332991) Ibrance	2015	CDK4/6	Estrogen receptor- and HER2-positive breast cancers
Pazopanib (GW786034) Votrient	2009	VEGFR1/2/3	RCC, soft tissue sarcomas
Pexidartinib (PLX3397) Turalio	2019	CSF1R	Tenosynovial giant cell tumors
Ponatinib (AP 24534) Iclusig	2012	BCR-Abl	Ph^+ CML or ALL
Regorafenib (GSK2118436) Tafinlar	2012	VEGFR1/2/3	Colorectal cancers
R406	2018	Syk	Chronic immune thrombocytopenia
Ribociclib (LEE011) Kisqali	2017	CDK4/6	Combination therapy with an aromatase inhibitor for breast cancers
Ruxolitinib (INCB-018424) Jakafi	2011	JAK1/2/3,Tyk	Myelofibrosis, polycythemia vera
Sirolimus (AY 22989) Rapamycin	1999	FKBP12/mTOR	Kidney transplants, lymphangioleiomyomatosis
Sorafenib (BAY 43–9006) Nexavar	2005	VEGFR1/2/3	HCC, RCC, thyroid cancer (differentiated)
Sunitinib (SU11248) Sutent	2006	VEGFR2	GIST, pancreatic neuroendocrine tumors, RCC
Temsirolimus (CCI-779) Torisel	2007	FKBP12/mTOR	RCC
Tofacitinib (CP-690550) Tasocitinib	2012	JAK3	Rheumatoid arthritis
Trametinib (GSK1120212) Mekinist	2013	MEK1/2	$BRAF^{V600E/K}$ melanomas, $BRAF^{V600E}$ NSCLC
Vandetanib (ZD6474) Zactima	2011	VEGFR2	Medullary thyroid cancers
Vemurafenib (PLX-4032) Zelboraf	2011	B-Raf	$BRAF^{V600E}$ melanomas

[a] Although many of these drugs are multikinase inhibitors, only the primary therapeutic targets are given here.
[b] ALL, acute lymphoblastic leukemias; AML, acute myelogenous leukemias; CLL, chronic lymphocytic leukemias; CML, chronic myelogenous leukemias; ErbB2/HER2, human epidermal growth factor receptor-2; GIST, gastrointestinal stromal tumors; HCC, hepatocellular carcinomas; NSCLC, non-small cell lung cancers; Ph^+, Philadelphia chromosome positive; RCC, renal cell carcinomas; SLL, small lymphocytic leukemias.

1. The importance of therapeutic protein kinase inhibitors

Because genetic alterations including mutations, overexpression, translocations, and dysregulation of protein kinases are involved in the pathogenesis of many illnesses including autoimmune, cardiovascular, inflammatory, and nervous diseases as well as cancer, this enzyme group has become one of the most important pharmaceutical targets over the past 20 years [1,2]. As much as 20–33 % of drug discovery efforts worldwide involve the protein kinase superfamily. The success of imatinib in the treatment of Philadelphia chromosome-positive chronic myelogenous leukemias and its FDA approval in 2001 fueled the interest in therapeutic protein kinase inhibitors [3]. The activated chimeric BCR-Abl protein-tyrosine kinase, which is inhibited by imatinib, is the chief biochemical defect that causes this leukemia.

The more than four thousand unique protein kinase structures in the public domain represent important aids in structure-based pharmaceutical development. Moreover, there are a greater number of proprietary structures within the pharmaceutical industry that are exploited in the drug discovery process. About 175 orally effective protein kinase inhibitors are in clinical trials worldwide [4]. A complete listing of these drugs, which is regularly updated, is found at www.icoa.fr/pkidb/. There are 52 FDA-approved therapeutics (see supplementary material) that target nearly 20 different protein kinases. Additional drugs targeting another 15–20 protein kinases are in clinical trials worldwide [4,5]. However, a total of 40 protein kinases represents only a small fraction of the 518-member protein kinase super family.

Manning et al. reported that the human protein kinase lineage contains 478 typical and 40 atypical enzymes [6]. These enzymes catalyze the following reaction;

$$MgATP^{1-} + protein\text{–}O\text{:}H \rightarrow protein\text{–}O\text{:}PO_3^{2-} + MgADP + H^+$$

Based upon the identity of the phosphorylated −OH groups, these enzymes are classified as protein-tyrosine kinases (90), protein-tyrosine kinase–like enzymes (43), and protein-serine/threonine kinases (385 members). The protein-tyrosine kinase group includes both receptor (58) and non-receptor (32) proteins. Moreover, this enzyme family includes a small group of catalysts such as MEK1/2 that mediate the phosphorylation of both threonine and tyrosine residues within the activation segment of target proteins; such enzymes are classified as dual specificity kinases. About one in 40 of all human genes encodes a protein kinase (518 protein kinase genes out of a total of 20,000 human genes). Accordingly, protein kinases constitute about 2.5 % of all human genes. Based upon chromosomal mapping, Manning et al. reported that 244 protein kinases map to cancer amplicons or disease loci [6]. These data portend a significant increase in the number of protein kinases that will be targeted for the treatment of many more illnesses.

The US FDA has approved a total of 52 small molecule protein kinase inhibitors as of 1 January 2020 (see supplementary material), nearly all of which are orally effective with the exception of temsirolimus (which is given intravenously) and netarsudil (an eye drop). Of the 52 approved drugs, eleven inhibit protein-serine/threonine protein kinases, two are directed against dual specificity protein kinases (MEK1/2), eleven block non-receptor protein-tyrosine kinases, and 28 target receptor protein-tyrosine kinases including the four fibroblast growth factor receptors, TRKA/B/C, ROS1, and CSF1R (Table 1). The data indicate that 46 of these drugs are prescribed for the treatment of neoplasms (41 against solid tumors including those of the breast, lung, and colon, and eight against non-solid tumors such as leukemias, and three against both solid and non-solid tumors: acalabrutinib, ibrutinib, and imatinib). At least 21 of the approved pharmaceuticals are multikinase inhibitors. This has potential advantages and drawbacks. It is possible that the therapeutic effectiveness of such drugs may be related to the inhibition of more than one enzyme. For example, cabozantinib and sunitinib have potent Axl off-target activity and this action may add to their clinical effectiveness [7]. In contrast, the inhibition of off-target enzymes may produce adverse side effects. Consequently, we have the problem of whether magic shotguns are to be preferred over magic bullets [8].

Eight of the currently approved protein kinase antagonists target non-malignancies. For example, fedratinib is employed for the treatment of myelofibrosis, ruxolitinib is used for the treatment of myelofibrosis and polycythemia vera, fostamatinib is prescribed for the treatment of chronic immune thrombocytopenia, baricitinib is employed for the treatment of rheumatoid arthritis, sirolimus is exploited for the treatment of renal graft vs. host disease, nintedanib is prescribed for the treatment of idiopathic pulmonary fibrosis, netarsudil is employed for the treatment of glaucoma, and tofacitinib is used for the treatment of rheumatoid arthritis, Crohn disease, and ulcerative colitis [9]. Moreover, sirolimus and ibrutinib are prescribed for the treatment of both neoplastic and non-neoplastic diseases.

Six drugs form covalent bonds with their target enzymes including afatinib (targeting EGFR in NSCLC), ibrutinib (inhibiting BTK in mantle cell lymphomas, chronic lymphocytic leukemias, marginal zone lymphomas, chronic graft vs. host disease, and Waldenström macroglobulinemia), osimertinib (targeting *EGFR T970M* mutants in NSCLC), acalabrutinib (inhibiting BTK in mantle cell lymphomas), neratinib (targeting ErbB2 in HER2-positive lung cancers), and dacomitinib (inhibiting mutant *EGFR* in lung cancers). The closely related *EGFR* and *ErbB4* are the most frequently mutated protein kinases in all cancers [3]. For a summary of the properties of small molecule protein kinase inhibitors that were approved by the FDA prior to 2019, see Ref. [9].

Of the 52 FDA-approved small molecule protein kinase inhibitors,

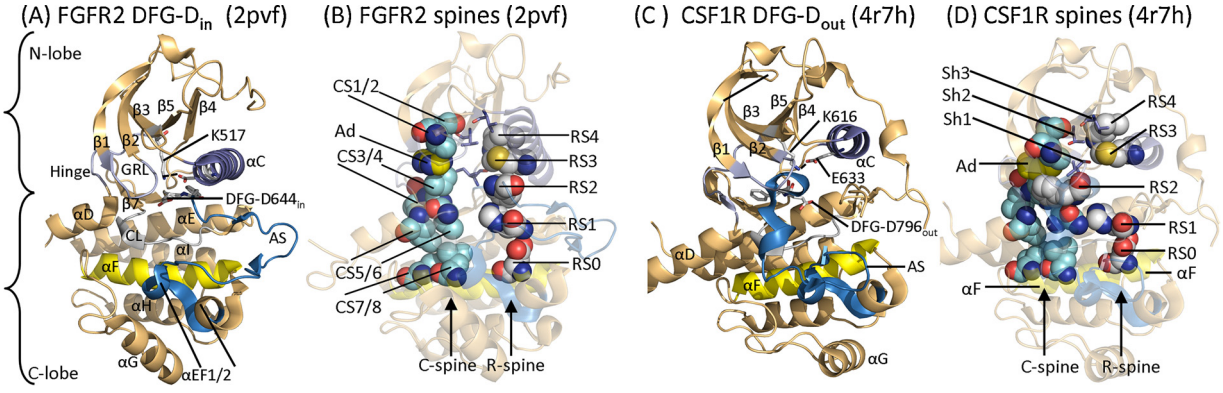

Fig. 1. (A) Structure of active FGFR2. (B) Structure of the C-spine and R-spine residues of active FGFR2 (spheres) and the shell residues (sticks). (C) The DFG-D$_{out}$ inactive form of CSF1R. (D) Spine and shell residues of inactive CSF1R. The carbon atoms of the C-spine are sky gray while those of the R-spine are cyan; the shell residues are shown in a stick format with carbon atoms in dark blue. The dashed lines represent a hydrogen bond. The PDB IDs are in parentheses. Ad, adenine; AS, activation segment; CL, catalytic loop; GRL, glycine-rich loop.

seventeen are used in the treatment of more than one disease. Imatinib, for example, is used in the treatment of eight disparate disorders (Table 1). Imatinib inhibits Abl (and BCR-Abl – responsible for the pathogenesis of chronic myelogenous leukemias), Abl2, PDGFRα/β, Kit (the stem cell factor receptor), epithelial discoidin domain-containing receptor-1 (DDR1), and discoidin domain-containing receptor-2 (DDR2), which makes it a multikinase inhibitor (ChEMBL ID: CHEMBL941). The latter two enzymes are activated by collagen and they participate in remodeling the extracellular matrix, cell differentiation, cell migration, and cell proliferation. The drug is FDA-approved for (i) the first-line treatment of Philadelphia chromosome-positive chronic myelogenous leukemias, (ii) *Kit* mutation-positive gastrointestinal stromal tumors, (iii) dermatofibrosarcoma protuberans, (iv) myelodysplastic/myeloproliferative diseases with *PDGFR* gene-rearrangements, (v) chronic eosinophilic leukemias, (vi) hypereosinophilic syndrome, and (vii) as a second-line treatment for aggressive systemic mastocytosis without the *KIT* ^{D816V} mutation and (viii) acute lymphoblastic leukemias [9]. Imatinib is thus a broad-spectrum inhibitor.

2. Protein kinase structure and mechanism

2.1. Primary, secondary, and tertiary structures

As first described by Knighton et al. for protein kinase A (PKA), protein kinases have a small N-terminal lobe and large C-terminal lobe [10,11]. The N-terminal lobe contains a five-stranded antiparallel β-sheet (β1–β5) and a regulatory αC-helix that occurs in active or inactive orientations [12,13]. The small lobe also contains a conserved glycine-rich (GxGxΦG) loop, sometimes called the P-loop, which occurs between the β1- and β2-strands; the Φ refers to a hydrophobic residue. A conserved valine residue follows the glycine-rich loop (GxGxΦGxV) and this valine interacts hydrophobically with the adenine base of ATP as well as many small molecule protein kinase inhibitors. A conserved AxK signature sequence is found within the β3-strand and a conserved glutamate is found near the middle of the αC-helix. The occurrence of an electrostatic bond between the β3-strand lysine and the αC-helix glutamate is found in active protein kinases and corresponds to the "αC_{in}" conformation (Fig. 1A). The αC_{in} conformation is necessary, but not sufficient, for the manifestation of full enzyme activity. However, the absence of this salt bridge indicates that the enzyme is inactive and this structure corresponds to the "αC_{out}" conformation. The conversion of the αC_{out} conformation to the αC_{in} conformation is required for the acquisition of catalytic activity.

The carboxyterminal lobe is predominantly α-helical with eight conserved helices (αD–αI, αEF1, αEF2) (Fig. 1A) [14]. The carboxyterminal lobe of functional protein kinases also contains four short β-strands (β6–β9). The second residue of the β7-strand, which occurs on the bottom of the adenine binding pocket, interacts hydrophobically with essentially all ATP-competitive protein kinase antagonists. The C-terminal lobe contains catalytic loop residues that assist in the transfer of the phosphoryl group from ATP to the protein substrates.

Hanks and Hunter described 12 subdomains (I–VIa, VIb–XI) that make up the functional core of protein kinases [15]. The K/E/D/D (Lys/Glu/Asp/Asp) motif plays a pivotal role in the catalytic action of virtually all active protein kinases. The *K* of *K*/E/D/D is the β3-strand lysine that forms salt bridges with the α- and β-phosphates of ATP (Fig. 2). The *E* of the K/*E*/D/D signature is the αC-helix glutamate that forms an electrostatic bond with the conserved β3-strand lysine. The catalytic-loop aspartate (the first *D* of K/E/*D*/D), which is a Lowry-Brönsted base (proton acceptor), plays a pivotal role during catalysis. Madhusudan et al. postulated that the catalytic-loop aspartate abstracts the proton from the protein substrate −OH group, which aids in the nucleophilic attack of oxygen with the ATP γ-phosphorus atom (Fig. 2) [16]. Furthermore, Zhou and Adams hypothesized that the catalytic-loop aspartate (HRD-D) positions the hydroxyl group of the protein substrate in a location that facilitates an in-line nucleophilic attack [17]. See Ref [18]. for a general overview of protein kinase enzymology and Table 2 for a list of the important residues in TRKA, FGFR1, CSF1R, and JAK2 (targets of the four kinase inhibitors approved by the FDA in 2019).

The second *D* of the K/E/D/*D* signature sequence represents the first residue of the activation segment. The activation segment of virtually all protein kinases begins with DFG and nearly all activation segments end with APE. The activation loop, which is generally 35–40 residues long, is a key structural and regulatory component in all protein kinases [19]. The activation loop mediates both protein substrate binding as well as overall catalytic efficiency. The primary structure of the catalytic loop of protein kinases is made up of HRD(x)$_4$N. The primary structure of the activation segment follows the catalytic loop. Two

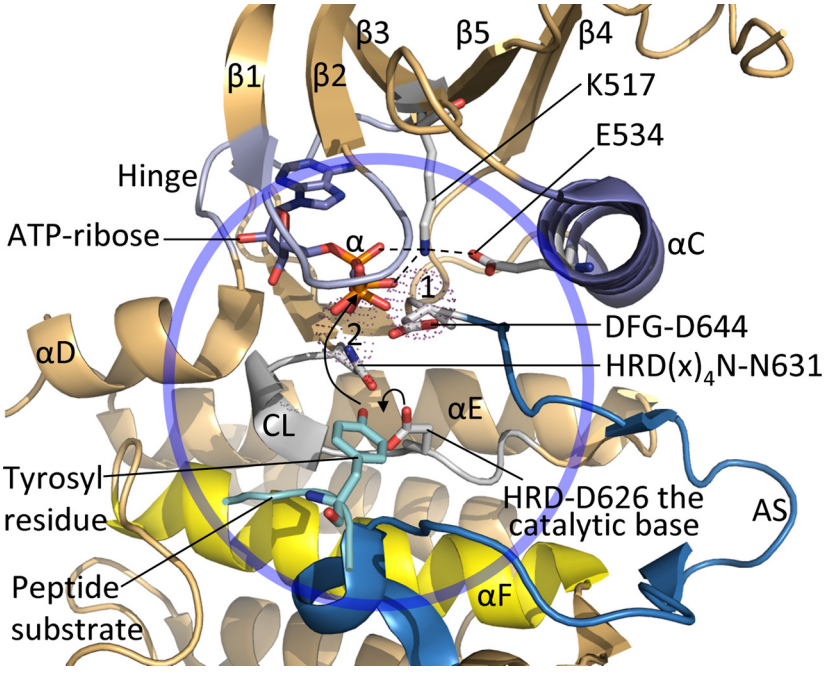

Fig. 2. Inferred mechanism of the FGFR2-catalyzed protein kinase reaction. HRD-D626 abstracts a proton from the peptidyl tyrosyl substrate allowing for its nucleophilic attack onto the γ-phosphorus atom of ATP. The two Mg^{2+} ions are shown as dots labeled 1 and 2. The chemistry occurs within the circle. AS, activation segment; CL, catalytic loop; The figure was prepared from FGFR2 (PDB ID: 2pvf).

Table 2
Important residues in selected human protein kinases.

	TRKA	FGFR1	CSF1R	JAK2
Number of residues	796	822	972	1132
Signal peptide	1–32	1–21	1–19	None
Extracellular segment	33–423	22–376	20–517	None
LRR1[a]	90–113	None	None	
LRR2[a]	116–137	None	None	
LRRCT[b]	148–193	None	None	
Ig-like domain 1	194–283	25–119	21–104	
Acid box	None	126–138	None	
Ig-like domain 2	299–365	158–246	107–197	
Ig-like domain 3	None	255–357	203–290	
Ig-like domain 4	None	None	299–399	
Ig-like domain 5	None	None	401–502	
Transmembrane segment	424–439	377–397	518–538	None
Intracellular segment	440–796	398–822	539–972	1132
Protein kinase domain	510–781	478–767	582–910	849–1142
Glycine-rich loop	^{517}GEGAFG^{522}	^{485}GEGCFG^{490}	^{589}GAGAFG^{595}	^{856}GKGNFG^{861}
The *K* of *K*/E/D/D, or the β3-lysine	544	514	616	882
β3-AxK	^{542}AVK^{544}	^{512}AVK^{514}	^{614}AVK^{616}	^{880}AVK^{882}
Molecular brake triad	None	N546, E562, K638	N648, E664, K793V	None
The *E* of K/*E*/D/D, the αC-glutamate	E560	531	633	898
Hinge-linker residues	^{590}EYMRHGD^{596}	^{562}EYASKGN^{568}	^{664}EYCTYGD^{670}	^{931}EYLPYGS^{936}
Gatekeeper residue	F589	V561	T663	M929
Kinase insert domain (KID)	606–619	580–594	682–749	None
Catalytic HRD-*D* residue, the first *D* of K/E/*D*/D	650	623	778	976
Catalytic loop *N* (HRD(x)$_4$*N*	655	628	783	981
Activation segment DFG-*D*, the second *D* of K/E/D/*D*	668	641	802	994
Activation segment tyrosine phosphorylation sites	676/680/681	653/4	809	1007, 1008
End of the activation segment	^{695}PPE^{697}	^{668}APE^{670}	^{823}APE^{825}	^{1022}APE^{1024}
Molecular weight (kDa)	87.5	91.9	108.0	130.6
UniProtKB ID	P04629	P11362	P07333	O60674

[a] LRR, leucine-rich repeat.
[b] LRRCT, leucine- rich repeat carboxyterminal.

Mg^{2+} ions, which are labeled Mg^{2+}(1) and Mg^{2+}(2), are needed for the catalytic activity of nearly all protein kinases (Fig. 2).

In terms of length and sequence, the center of the activation segment varies greatly among all protein kinases [1]. The activation segment in most protein kinases contains one or more phosphorylatable residues. Moreover, activation segment phosphorylation is required for full enzyme activity in most, but not all, protein kinases. For example, ErbB1/2/4 of the EGFR family exhibit full activity in the absence of phosphorylation. The beginning of the activation segment is found near the conserved HRD signature of the catalytic loop and the amino-terminus of the αC-helix. Although the αC-helix occurs within the N-terminal lobe, it occupies a strategically important position between the small and large lobes.

The activation segment of protein kinases exhibits an extended or open configuration in all active protein kinases (Fig. 1A) and a closed configuration in most dormant enzymes (Fig. 1C) [1]. The initial two residues of the activation segment are found in two different conformations. The DFG-D side chain of functional and active protein kinases is directed toward the ATP-binding site and it coordinates Mg^{2+}(1). This conformation is called the "DFG-D_{in}" structure (Fig. 1A). In the dormant activation segment configuration observed in many protein kinases, the DFG-D is directed away from the ATP-binding site. This conformation is called the "DFG-D_{out}" structure (Fig. 1C). It is the capacity of the DFG-D aspartate to bind (DFG-D_{in}) or not bind (DFG-D_{out}) to Mg^{2+}(1) within the active site that is important. See Ref. [1] for more material about these two activation segment structures.

2.2. Protein kinase hydrophobic skeletons

Kornev et al. examined the tertiary structures of active and inactive conformations of about two dozen protein kinases to determine the identity of structurally and functionally important residues [20,21]. Their studies revealed a composite of eight amino acids that form a catalytic spine (C-spine) and four amino acid residues that form a regulatory spine (R-spine). Residues from both lobes are found in each of these spines. These spinal structures make up a stable, but flexible, assembly that is functionally important. The C-spine positions ATP for catalysis and the R-spine positions the protein substrate. The R-spine contains residues from both the αC-helix and the activation segment, whose locations and structures are important in determining active and dormant enzyme states. The accurate alignment and positioning of both spines are necessary, but not sufficient, for the formation of a catalytically active protein kinase.

The R-spine consists of the initial residue of the β4-strand and a residue near the C-terminal end of the αC-helix, both within the small lobe [20]. This spine also contains the activation segment DFG-phenylalanine (DFG-F) and the catalytic loop HRD-histidine (HRD-H), both in the large lobe. The R-spine residue within the αC-helix is four residues carboxyterminal to the conserved αC-helix glutamate. The backbone N−H group of HRD-H forms a hydrogen bond with the side chain of a conserved aspartate residue in the αF-helix. From the bottom to the top, Meharena et al. designated the R-spine residues as RS0, RS1, RS2, RS3, and RS4 [22]. We later designated the catalytic spine residues as CS1–8, from the bottom to the top (Fig. 1B and D) [23]. The spine and shell residues of TRKA, FGFR1, CSF1R, and JAK2 are listed in Table 3.

The importance of the interaction of therapeutic protein kinase antagonists with the R-spine, the C-spine, and the shell residues is widespread and cannot be overstated. For a listing of the properties of the spine and shell residues of the EGFR family of protein-tyrosine kinases see Refs. [24–26], for the PDGFRα/β protein-tyrosine kinases see [27], for the VEGFR1/2/3 protein-tyrosine kinases see [28], for the Kit receptor protein-tyrosine kinase see [29], for the ROS1 orphan receptor protein-tyrosine kinase see [30], for the RET receptor protein-tyrosine kinase see [31], for the ALK receptor protein-tyrosine kinase see Refs. [32,33], for the fibroblast growth factor receptor protein-tyrosine

Table 3
Human TRKA, FGFR1, CSF1R and JAK2 R-spine, C-spine and Shell residues.

		KLIFS No.[a]	TRKA	FGFR1	CSF1R	JAK2
Regulatory spine						
β4-strand (N-lobe)	RS4	38	F575	L547	L649	Y913
C-helix (N-lobe)	RS3	28	L564	M535	M637	L902
Activation loop (C-lobe) F of DFG	RS2	82	F669	F642	F797	F995
Catalytic loop His (C-lobe)	RS1	68	H648	H621	H776	H974
F-helix (C-lobe)	RS0	None	D709	D682	D837	D1036
R-shell						
Two residues upstream from the gatekeeper	Sh3	43	M587	V559	V661	L927
Gatekeeper, end of β5-strand	Sh2	45	F589	V561	T663	M929
αC-β4 loop	Sh1	36	V573	I545	V647	V911
Catalytic spine						
β3-AxK motif (N-lobe)	CS8	15	A542	A512	A614	V863
β2-strand (N-lobe)	CS7	11	V524	V492	V596	A880
β7-strand (C-lobe)	CS6	77	L657	L630	L785	L983
β7-strand (C-lobe)	CS5	78	V658	V631	L786	V984
β7-strand (C-lobe)	CS4	76	C656	V629	V784	I982
D-helix (C-lobe)	CS3	53	L597	L569	L671	L937
F-helix (C-lobe)	CS2	None	V716	L689	L844	V1043
F-helix (C-lobe)	CS1	None	I720	I693	I848	L1047

[a] From Refs. [3,50].

kinases, see Ref. [34], for the Janus kinase non-receptor protein-tyrosine kinases see [35], for the CDK (cyclin-dependent kinase) lineage of protein/serine kinases see [14,36], for the Raf protein-serine/threonine kinases see [37], for the ERK1/2 protein-serine/threonine kinases see [38,39], for the MEK1/2 dual-specificity protein kinases see [40], and for the Src non-receptor protein-tyrosine kinase see [41].

The protein kinase catalytic spine is made up of two residues from the small lobe and six residues from the large lobe. The binding of the adenine base of ATP couples the two parts of the catalytic spine together and this interaction enables the closure of the two lobes of the enzyme (Fig. 1B and D) [21]. This completion of the catalytic spine by binding ATP prepares the enzyme for catalysis. The two residues of the N-terminal lobe that bind to the nucleotide substrate adenine include the conserved valine in the β2-strand following the glycine-rich loop GxGxΦGxV (CS7) and the conserved alanine (CS8) from the AxK motif of the β3-strand. Moreover, CS6 in the middle of the β7-strand of the carboxyterminal lobe interacts hydrophobically with the adenine moiety of ATP. CS4 and CS5 interact with CS3 at the beginning of the αD-helix. Additionally, CS3 interacts hydrophobically with the neighboring CS4 as well as CS1 of the αF-helix below it. Both the R- and C-spines are buttressed by the hydrophobic αF-helix, which serves as a dominant underpinning for the assembly and stabilization of the entire protein kinase domain. The hinge region of protein kinases connects the amino-terminal and carboxyterminal lobes of protein kinases and the 6-amino group of ATP generally forms a hydrogen bond with the carbonyl backbone of the first hinge residue. Furthermore, the adenine *N*1 of ATP generally forms a hydrogen bond with the backbone N−H group of the third hinge residue. Nearly all small-molecule steady-state ATP competitive inhibitors of protein kinases also make hydrogen bonds with the backbone residues of the hinge, most commonly with the third hinge residue [23].

Using the results of site-directed mutagenesis studies, Meharena et al. detected three residues in murine protein kinase A that fortify the R-spine, which they designated as Sh1, Sh2, and Sh3 where Sh refers to shell [22]. While their Sh1 V104 G mutant had 5 % of the catalytic activity of wild type PKA, their M118 G/M120 G Sh3/Sh2 double mutant was kinase dead. These results demonstrate that the shell residues significantly stabilize the PKA structure. It is likely that the shell residues play a similar stabilizing role in all protein kinases. The Sh1 residue occurs within the αC-β4 back loop. The Sh2 or gatekeeper residue is found at the end of the β5-strand and it occurs immediately before the hinge region while the Sh3 residue occurs two residues upstream from the Sh2 gatekeeper within the β5-strand (Fig. 1D).

The name gatekeeper reflects the role that this amino acid plays in regulating access to the hydrophobic pocket contiguous with the adenine binding pocket [42,43] that is occupied by structural fragments of various small molecule protein kinase blockers. Based upon the findings of Meharena et al. [22], only three of the 14 amino acids adjacent to RS3 and RS4 in protein kinase A are conserved. To reiterate, many therapeutic steady-state ATP-competitive small molecule protein kinase antagonists interact with the R-spine (RS2/3) C-spine (CS6/7/8), and shell (Sh1 and Sh2) residues. Ung et al. found that about 77 % of protein kinases have a relatively large gatekeeper residue (e.g., Phe, Leu, Met) while the rest have smaller gatekeeper residues (e.g., Val, Thr) [44].

3. Inhibitor classification

Dar and Shokat classified protein kinase blockers into three groups, which they designated as types I, II, and III [43]. They defined type I inhibitors as those that bind within and around the adenine pocket of a catalytically active protein kinase. Furthermore, they defined type II inhibitors as those that bind to a dormant DFG-D_{out} protein kinase while type III inhibitors bind to an allosteric site that does not overlap the adenine-binding pocket. Additionally, Zuccotto defined type I½ inhibitors as those pharmaceuticals that bind to a dormant protein kinase with a DFG-D_{in} structure [45]. Such a dormant protein kinase may display a non-linear or broken R-spine, an αC_{out} conformation, a closed activation segment, an autoinhibitory brake, an abnormal glycine-rich

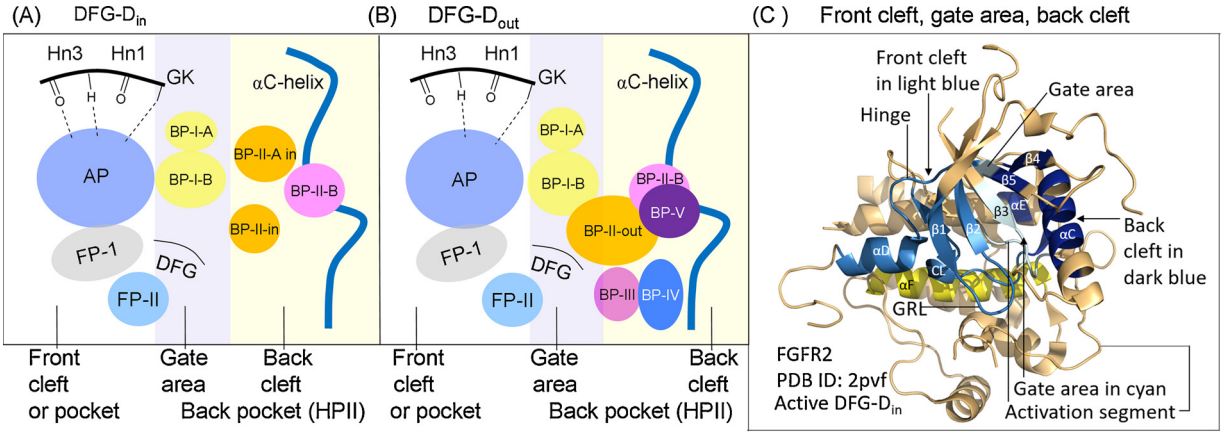

Fig. 3. (A and B) Location of the protein kinase domain drug-binding pockets. Adapted from Refs. [50,51]. (C) Location of the protein kinase front cleft, gate area, and back cleft. AP, adenine pocket; BP, back pocket; FP, front pocket; Hn, hinge; HPII, hydrophobic pocket II; GK, gatekeeper.

loop, or various combinations of these structural parameters. Later, Gavrin and Saiah divided allosteric inhibitors into types III and IV [46]. Type III inhibitors bind within the deep cleft separating the amino-terminal and carboxyterminal lobes and adjacent to, but independent of, the ATP binding site. Contrariwise, type IV inhibitors bind outside of the cleft. Moreover, Lamba and Gosh defined agents that span two distinct regions of the protein kinase domain as type V or bivalent inhibitors [47]. For example, a ligand that binds to (i) the adenine-binding pocket and (ii) the SH2 domain of Src would be classified as a type V inhibitor [48]. For completion, we classified type VI inhibitors as those compounds that form a covalent bond with their target enzyme [23]. For example, afatinib is a type VI inhibitor that covalently binds to mutant *EGFR* and is prescribed for the treatment of NSCLC. Mechanistically, this therapeutic initially binds like a type I inhibitor to an active EGFR structure and then the C797 –SH group of the enzyme attacks the drug and forms a covalent Michael adduct (PDB ID: 4g5j) [23].

We have divided type I½ and type II inhibitors into A and B subtypes [23]. Type A antagonists are pharmaceuticals that extend past the Sh2 gatekeeper residue into the back cleft. In contrast, type B inhibitors are pharmaceuticals that fail to extend into the back cleft. Based upon preliminary findings, the possible importance of this difference is that type A inhibitors bind to their target enzyme with longer residence times [49] as compared with type B inhibitors [23]. Sorafenib is a type IIA VEGFR antagonist that is approved by the FDA for the treatment of renal cell carcinomas. Sunitinib is a type IIB VEGFR inhibitor that is also approved by the FDA for the treatment of renal cell carcinomas. The type IIA inhibitor has a residence time greater than 64 min [23] while that of the type IIB inhibitor has a residence time of less than 2.9 min [49].

4. Drug binding pockets

van Linden et al. [50] and Liao [51] divided the region between the amino-terminal and carboxyterminal lobes of protein kinases into the front cleft (front pocket), the gate area, and the back cleft. A general overview depicting these locations and various sub-pockets is provided in Fig. 3 and Table 4. The gate area and back cleft constitute HPII (hydrophobic pocket II) or the back pocket. The front cleft includes the last three residues of the β1-strand, the glycine-rich loop, the first four residues of the β2-strand, the hinge region and linker, the αD-strand, the catalytic loop, and the β7-strand. Type I inhibitors characteristically target the front cleft. The gate area consists of the three residues at the end of the β3-strand and the first two residues of the β3-αC loop, the residue immediately before the activation segment, and the first four residues of the activation segment. The back cleft consists of the middle of the αC-helix, the β4-strand, the last two residues of the β5-strand, the first two and fifth residues from the αE-helix, and the two residues preceding the catalytic loop (Fig. 3C). Many type I½ inhibitors occupy both the front cleft and part of the back cleft. One of the prospective goals in the design of small molecule protein kinase pharmaceuticals is to achieve selectivity in order to reduce off-target side effects [52]; this process is assisted by comparing drug interactions with their target enzymes [5,53,54]. Designing drug scaffold appendages that bind to residues lining the pockets or sub-pockets within the cleft plays a strategic role in protein kinase inhibitor drug development and discovery with the goal of maximizing drug affinity.

van Linden et al. established a comprehensive catalog of drug and ligand binding to more than twelve hundred human and mouse protein kinases [50]. The KLIFS (kinase–ligand interaction fingerprint and structure) catalog includes an arrangement of 85 possible ligand binding-site residues that are found in both lobes [3]. The listing helps in the discovery of related interactions and facilitates the classification of ligands and drugs based upon their binding characteristics. Furthermore, these authors devised a universal amino acid residue numbering system that aids in the comparison of different drug-kinase interactions [50]. Table 3 lists the correspondence between the R-spine, C-spine, and shell residue numbers and the KLIFS database residue nomenclature. Additionally, these investigators launched a useful non-commercial and searchable web site, which is regularly updated, that describes the interaction of human and mouse protein kinases with bound drugs and ligands (klifs.vu-compmedchem.nl/). Furthermore, the BRIMR (Blue Ridge Institute for Medical Research) website, which is also regularly updated, depicts the structures and the Lipinski rule of five properties [55] of all small molecule protein kinase inhibitors that are approved by the US FDA (www.brimr.org/PKI/PKIs.htm). Moreover, Carles et al. prepared a comprehensive directory of small molecule protein kinase and PI3K antagonists that have been or are in clinical trials [4]. They developed a non-commercial and searchable web site, which is also regularly updated, that includes inhibitor physicochemical structures and properties, their enzyme targets, their therapeutic indications, the year of first approval (if applicable), and their trade names (http://www.icoa.fr/pkidb/).

5. Drug-enzyme interactions

Entrectinib is an indazole derivative (Fig. 4A) [56] that was approved in 2019 for the treatment of adult and pediatric patients 12 years of age or older with solid tumors that have a neurotrophic receptor protein-tyrosine kinase (NTRK1/2/3) gene fusion without a known resistance mutation [57]. These three genes encode the TRKA/B/C neurotrophin receptor protein tyrosine kinases. Nerve growth factor (NGF) is the chief ligand that stimulates TRKA; the *NGF* gene encodes a 241-residue polypeptide that is processed to yield a 120-residue growth factor. Moreover, brain-derived neurotrophic factor (BDNF) or neurotrophin-4 (NT-4) is the main TRKB stimulatory ligand; the *NTF4* gene encodes a 210-residue polypeptide that is processed to yield a 130-residue growth factor. Additionally, neurotrophin-3 is the chief TRKC stimulatory ligand; the *NTF3* gene encodes a 257-residue polypeptide that is processed to yield a 119-residue growth factor [58].

The formation of NTRK1/2/3 chimeric fusion proteins is the most common mechanism of oncogenic TRKA/B/C activation [58]. Chromosomal rearrangements result in the formation of hybrid genes in which the 5′ sequences of the fusion partner are juxtaposed to the 3′ sequences of *NTRK1/2/3*. The product of such fusions is a chimeric oncoprotein that exhibits ligand-independent activation of the TRK protein kinase. The upstream partners usually contain structures such as zinc-finger domains, WD repeats, or coiled-coil domains that readily dimerize. Zinc finger domains include IRF2BP2 and TRAF2; WD domains include RFWD2, STRN, and EML4. There are at least a dozen fusion proteins with the coiled-coil domain including MPRIP, TFG, TRIM24, and TMP4. These TRK fusion proteins signal through the same downstream pathways as those that are activated by full length TRKA/

Table 4
Location of selected catalytic cleft residues.

Description	Location	KLIFS residue no.[a]
GxGxΦG	Front cleft	4–9
β2-strand V (CS7)	Front cleft	11
β3-strand A (CS8)	Front cleft	15
HRD with DFG-D_{in}	Front cleft	68–70
$HRD(x)_4N$-N	Front cleft	75
β7-strand CS6	Front cleft	77
β3-strand K; three residues before the αC-helix	Gate area	17
αC-β4 penultimate back loop residue	Gate area	36
Gatekeeper	Gate area	45
The x of xDFG	Gate area	80
DFG	Gate area	81–83
αC-helix E	Back cleft	24
RS3	Back cleft	28
HRD with DFG-D_{out}	Back cleft	68–70

[a] Ref. [50].

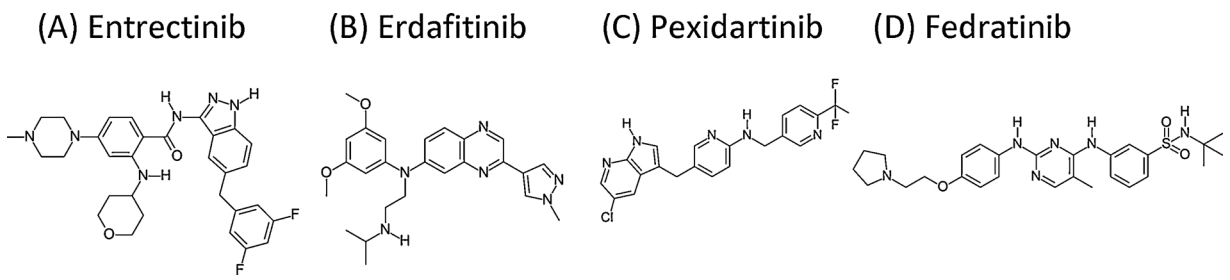

Fig. 4. Structures of the small molecule protein kinase antagonists approved by the FDA in 2019.

B/C proteins including the MAP kinase, PKB/Akt, and phospholipase C pathways. Based upon nearly 34,000 analyses, Solomon et al. reported that the incidence of *NTRK1/2/3* fusion proteins in salivary gland carcinomas was about 5 %, that of thyroid carcinomas was about 2.3 %, and that of inflammatory fibroblastic tumors was about 18 % [59]. The percentage of these fusion proteins in other neoplasms was much lower: breast carcinomas (0.13 %), lung adenocarcinomas (0.23 %), colorectal carcinomas (0.31 %), pancreatic adenocarcinomas (0.34 %), melanomas (0.36 %), cholangiocarcinomas (0.25 %), neuroendocrine tumors (0.31 %), and sarcomas (0.68 %)

Entrectinib is used for the treatment of any cancer harboring the gene fusion protein regardless of the organ, tissue, anatomical location, or histology type; it is thus tissue agnostic. The overall response rate for patients with NTRK fusion proteins receiving entrectinib was 57 % [60]. Larotrectinib is the only other protein kinase antagonist that is tissue agnostic and it is also approved for the treatment of patients with NTRK1/2/3 gene fusions [61,62]. There have been no direct head-to-head comparisons of the relative effectiveness of these two drugs in the treatment of neoplasms associated with these gene fusions. Entrectinib was also approved in 2019 for the treatment of ROS1-positive NSCLC [60]. The overall response rate in this group of patients was 55 %. Unlike crizotinib, which is approved for the treatment of this cancer, entrectinib readily penetrates the blood-brain barrier and it is effective in patients with ROS1-positive metastatic NSCLC brain metastases. The IC_{50} values of entrectinib for TRKA/B/C, ROS1, and ALK are 1/3/5, 12, and 7 nM, respectively. Entrectinib is thus a potent inhibitor of these enzyme targets.

The X-ray crystal structure of entrectinib bound to TRKA shows that the *N*1 N−H group of the indazole forms a hydrogen bond with E590 and *N*2 forms a hydrogen bond with the backbone amide of M592 and the amino group of the drug forms a hydrogen bond with the carbonyl backbone of M592 (the third hinge residue) (Fig. 5A). The drug makes hydrophobic contact with four spine residues (CS5/6/7/8) and two shell residues (Sh1/2) (Table 5). The therapeutic interacts hydrophobically with the β1-strand residue that is proximal to the glycine-rich loop (L516); this residue is equivalent to KLIFS-3 (kinase–ligand interaction fingerprint and structure residue-3). Entrectinib also makes hydrophobic contact with E518 within the glycine-rich loop, the F589 gatekeeper residue, R593, H594, D596 within the hinge, R599 within the αD-helix, R654, N655 within the catalytic loop, and DFG-D668. The drug occupies the front pocket and FP−I; it does not extend into or past the gate area. The enzyme has an inactive DFG-D_{in} conformation with a closed activation segment and the drug-enzyme complex corresponds to that of a type I½B inhibitor [23]. Although clinical experience with entrectinib is limited, resistance mechanisms following the treatment of fusion-protein driven malignancies have already been described [58]. These include a G595R mutation within the hinge and a G667C mutation corresponding to the x residue of xDFG in TRKA. The former mutation may be inhibitory owing to the steric hindrance of drug binding. The latter mutation occurs proximally to the important activation segment, but it is unclear how the introduction of the rather small cysteine in place of glycine could block entrectinib binding.

Erdafitinib is a quinoxaline derivative (Fig. 4B) [63] that was approved in 2019 for the second-line treatment of unresectable or metastatic urinary bladder cancer following platinum-based chemotherapy or for the first-line treatment of urothelial bladder cancers bearing susceptible *FGFR2/3* gene alterations [64]. Loriot et al. reported that the response rate to second-line erdafitinib therapy in patients with *FGFR2/3* fusion proteins or *FGFR3* mutations was 40 % with 37 % achieving a partial response and 3 % achieving a full response [63]. The IC_{50} values for FGFR1/2/3/4 are 2.0/2.0/4.0/6.3 nM and that for VEGFR2 is 50 nM. Accordingly, erdafitinib is classified as a pan-FGFR inhibitor. The X-ray crystal structure shows that the *N*1 of quinoxaline forms a hydrogen bond with A564 (the third hinge residue) and the dimethoxyphenyl oxygen forms a hydrogen bond with the N−H group of FGFR1 DFG-D641 (Fig. 5B) [65]. Erdafitinib makes hydrophobic contact with five spine residues (RS2/3, CS6/7/8), all three shell residues (Sh1/2/3), and the KLIFS-3 residue (Table 5). Erdafitinib also makes hydrophobic contact with the AVK514 of the signature sequence of the β3-strand, I545 of the αC-β4 back loop, E562, Y563, A564, and S565 within the hinge, $HRD(x)_4N628$, and A640 (the x of xDFG). Moreover, erdafitinib occupies the front cleft, gate area, back cleft, FP-I,

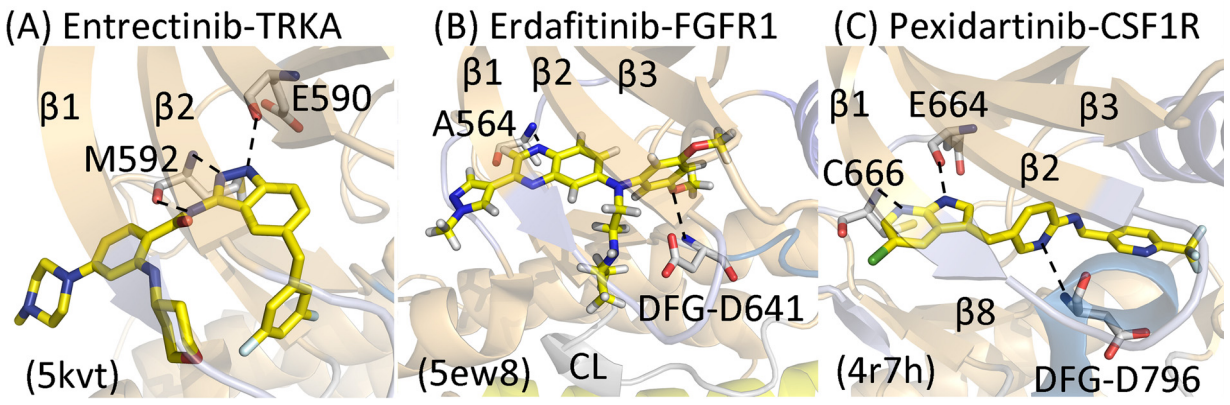

Fig. 5. Structures of drug-enzyme complexes. The dashed lines depict hydrogen bonds. The corresponding PDB ID files are within parentheses. CL, catalytic loop.

Table 5
Drug-enzyme hydrophobic (Φ) and hydrogen bonding (HB) interactions based upon their common KLIFS residue numbers[a,b].

	PDB ID	RS1	RS2	RS3	RS4	Sh1	Sh2	Sh3	CS5	CS6	CS7	CS8	KLIFS-3[c]	KLIFS pockets[a]
KLIFS no. →		68	82	28	38	36	45	43	76	77	11	15	3	
Drug-enzyme ↓														
Type I inhibitors														
Bosutinib-Src	4mxo			Φ		Φ	Φ	Φ		Φ	Φ	Φ	Φ	F,G, BP-I-A/B
Brigatinib-ALK	6mx8			Φ,HB			Φ			Φ	Φ	Φ	Φ	F, FP-I
Crizotinib-ROS	3zbf					Φ	Φ			Φ	Φ	Φ	Φ	F, FP-I
Dasatinib-Abl	2gqg			Φ		Φ	Φ,HB	Φ		Φ	Φ	Φ	Φ	F, G, B, BP-I-A/B
Erlotinib-EGFR	1m17						Φ	Φ		Φ	Φ	Φ	Φ	F, G, B, BP-I-A/B
Gefitinib-EGFR	2ity			Φ			Φ	Φ		Φ	Φ	Φ	Φ	F,G, BP-I-A/B
Palbociclib-CDK6	2euf					Φ	Φ			Φ	Φ	Φ	Φ	F
R406 (fostamatinib)	3fqs					Φ	Φ			Φ	Φ	Φ	Φ	F
Tofacitinib-JAK1	3eyg					Φ	Φ			Φ	Φ	Φ	Φ	F, FP-I/II
Tofacitinib-JAK3	3lxk					Φ	Φ		Φ	Φ	Φ	Φ	Φ	F, FP-I/II
Vandetanib-RET	2ivu				Φ	Φ	Φ	Φ		Φ	Φ	Φ	Φ	F,G, BP-I-A/B
Type I½A inhibitors														
Dabrafenib–B-Raf	5csw		Φ,HB	Φ	Φ	Φ	Φ	Φ		Φ	Φ	Φ	Φ	F, G, B, BP-I-A/B, BP-II-in, BP-II-A-in
Erdafitinib-FGFR1	5ew8		Φ	Φ		Φ	Φ	Φ		Φ	Φ	Φ	Φ	F, G, B, FP-I, BP-I-A/B
Lapatinib-EGFR	1xkk		Φ	Φ	Φ	Φ	Φ	Φ		Φ	Φ	Φ	Φ	F, G, B, BP-I-A/B, BP-II-in, BP-II-A-in
Lenvatinib-VEGFR	3wzd		Φ	Φ		Φ	Φ			Φ	Φ	Φ	Φ	F, G, B, BP-I-B, BP-II-in
Palbociclib-CDK6	5l2i					Φ	Φ			Φ	Φ	Φ	Φ	F
Vemurafenib-B-Raf	3og7		Φ	Φ	Φ	Φ	Φ	Φ		Φ	Φ	Φ	Φ	F, G, B, FP-I, BP-I-A/B, BP-II-in, BP-II-A-in
Type I½B inhibitors														
Abemeciclib-CDK6	5l2s					Φ	Φ			Φ	Φ	Φ	Φ	F, FP-II
Alectinib-ALK	3aox					Φ	Φ			Φ	Φ	Φ	Φ	F, BP-I-B
Ceritinib-ALK	4mkc			Φ,HB		Φ				Φ	Φ	Φ	Φ	F, FP-I
Crizotinib-ALK	2xp2			Φ			Φ			Φ	Φ	Φ	Φ	F, FP-I
Crizotinib-Met	2wgj			Φ,HB		Φ	Φ			Φ	Φ	Φ	Φ	F, FP-I
Entrectinib-TRKA	5kvt					Φ	Φ		Φ	Φ	Φ	Φ	Φ	F, FP-I
Erlotinib-EGFR	4hjo			Φ,HB		Φ	Φ			Φ	Φ	Φ	Φ	F, G, BP-I-A/B
Ribociclib-CDK6	5l2t			HB		Φ	Φ			Φ	Φ	Φ	Φ	F, G, FP-I
Type IIA inhibitors														
Axitinib-VEGFR	4ag8		Φ	Φ		Φ	Φ	Φ		Φ	Φ	Φ	Φ	F, G, B, BP-I-B, BP-II-out
Imatinib-Abl[d]	1iep	Φ,HB	Φ	Φ		Φ	Φ,HB	Φ		Φ	Φ	Φ	Φ	F, G, B, BP-I-A/B, BP-II-out, BP-IV
Imatinib-Kit	1t46	Φ	Φ	Φ		Φ	Φ,HB	Φ		Φ	Φ	Φ	Φ	F, G, B, BP-I-A/B, BP-II-out, BP-IV
Nilotinib-Abl	3cs9	Φ	Φ	Φ		Φ	Φ,HB	Φ		Φ	Φ	Φ	Φ	F, G, B, BP-I-A/B, BP-II-out, BP-V
Pexidartinib-CSF1R	4r7h		Φ	Φ		Φ	Φ			Φ	Φ	Φ	Φ	F, G, B, BP-I-B, BP-II-out, BP-V
Ponatinib-Abl[d]	3oxz	Φ,HB	Φ	Φ		Φ	Φ	Φ		Φ	Φ	Φ	Φ	F, G, B, BP-I-A/B, BP-II-out, BP-III, BP-IV
Ponatinib-Kit	4u0i	Φ,HB	Φ	Φ		Φ	Φ	Φ		Φ	Φ	Φ	Φ	F, G, B, BP-II-A/B, BP-II-out, BP-III, BP-IV
Ponatinib-B-Raf	1uwh	Φ	Φ	Φ		Φ	Φ			Φ	Φ	Φ	Φ	F, G, B, BP-I-B, BP-II-out, BP-III
Sorafenib-CDK8	3rgf	Φ	Φ	Φ		Φ	Φ			Φ	Φ	Φ	Φ	F, G, B, BP-I-B, BP-II-out, BP-III
Sorafenib-VEGFR	4asd	Φ	Φ	Φ		Φ	Φ			Φ	Φ	Φ	Φ	F, G, B, BP-I-B, BP-II-out, BP-III
Type IIB inhibitors														
Bosutinib-Abl	3ue4		Φ	Φ		Φ	Φ	Φ		Φ	Φ	Φ	Φ	F, G, BP-II-A/B
Sunitinib-Kit	3g0e		Φ			Φ				Φ	Φ	Φ	Φ	F
Sunitinib-VEGFR	4agd		Φ			Φ	Φ			Φ	Φ	Φ	Φ	F, BP-I-B
Type III and VI inhibitors														
Cobimetinib-MEK1	4an2		Φ	Φ		Φ	Φ	Φ		Φ	Φ	Φ	Φ	F, G, B, BP-II-in
Afatinib-EGFR	4g5j			Φ			Φ	Φ		Φ	Φ	Φ	Φ	F, G, BP-II-A/B
Ibrutinib-BTK	5p9j		Φ	Φ		Φ	Φ	Φ		Φ	Φ	Φ	Φ	F, G, B, BP-I-B

[a] klifs.vu-compmedchem.nl/.
[b] Human enzyme unless otherwise noted.
[c] KLIFS-3, kinase-ligand interaction fingerprint and structure residue-3.
[d] Mouse enzyme.

BP-I-A, and BP-I-B and it extends past the gatekeeper residue. The compound is bound to a DFG-D_{in} inactive conformation of FGFR1 with the activation segment in a closed conformation and an engaged autoinhibitory brake [34]. Overall this interaction corresponds to that of a type I½A inhibitor [23].

Hyperphosphatemia occurs in about three-quarters of the patients receiving erdafitinib and it is one of its most common side effects [63,64]. FGF23 is an important factor in the regulation of phosphate homeostasis. FGF23 is released from the bone under physiological conditions and suppresses phosphate reabsorption in the proximal tubules of the kidney [66]. Inhibiting the action of FGF23 allows phosphate reabsorption to occur thereby leading to hyperphosphatemia. It has been hypothesized that FGFR1 is a major participant in renal phosphate homeostasis [67,68]; however, this is not entirely settled and it may also involve the participation of FGFR3/4 [69]. Chronically elevated serum phosphate often leads to ectopic calcifications in soft tissues. Elevated serum phosphate represents a biomarker for FGFR inhibition; moreover, it is class specific and it mirrors the inhibition of FGF23 action and not that of other growth factors nor their corresponding receptor protein kinases. Loriot et al. reported that Grade 3 (out of 4) hyponatremia occurs in about 11 % of patients treated with erdafitinib [63] and the mechanism of this response is unclear. See Refs [64,70]. for a summary of the clinical trials that led to the approval of erdafitinib.

Pexidartinib is a pyrrolo[2,3-*b*]pyridine derivative (Fig. 4C) that was approved in 2019 for the treatment of adult patients with tenosynovial giant cell tumors associated with severe morbidity or functional limitations and not amenable to improvement with surgery [71]. These rare but aggressive neoplasms commonly arise in the synovium of joints or tendon sheaths of young adults. The non-malignant neoplastic cells often express colony-stimulating factor 1 (CSF1) and they commonly have a t(1;2) translocation that links the *CSF1* gene on chromosome

1p13 to the *COL6A3* gene on chromosome 2q35. Pexidartinib inhibition of CSF1 and CSF1R signaling thus targets the underlying cause of the disease. The IC_{50} values of pexidartinib for CSF1R, Kit, and VEGFR2 are 17, 12, and 210 nM, respectively. Pexidartinib can produce serious and potentially fatal liver injury and liver function tests are performed prior to initiating treatment. In a clinical trial involving patients with the giant cell tumors, the overall response rate was 40 %, the complete response rate was 15 %, the partial response rate was 25 %, and the placebo response rate was 0 %. The pharmaceutical is currently in a number of clinical trials as a single agent or in combination with other drugs for the treatment of a variety of solid tumors. See Ref. [72] for a summary of the ENLIVEN clinical trial results of pexidartinib vs. placebo in the treatment of tenosynovial giant cell tumors.

The X-ray crystal structure of pexidartinib bound to CSF1R (Fig. 5C) shows that the pyrrolo N—H group forms a hydrogen bond with the carbonyl backbone of E664 and the pyridine nitrogen forms a hydrogen bond with the N—H group of C666 (the third hinge residue). Moreover, one of the pyridine nitrogen atoms forms a hydrogen bond with the

Table 6
Properties of FDA-approved small molecule inhibitors[a].

Drug	PubMED CID	Formula	MW (Da)	HD[b]	HA[c]	cLogP[a,d]	Rotatable bonds	PSA[e] (Å^2)	Ring count	Complexity[f]
Abemaciclib	46220502	$C_{27}H_{32}F_2N_8$	507	1	9	5.2	7	75	5	723
Acalabrutinib	71226662	$C_{26}H_{23}N_7O_2$	466	2	6	1.1	4	119	5	845
Afatinib	10184653	$C_{24}H_{25}ClFN_5O_3$	486	2	8	4.0	8	88.6	4	702
Alectinib	49806720	$C_{30}H_{34}N_4O_2$	483	1	5	4.7	3	72.4	6	867
Axitinib	6450551	$C_{22}H_{18}N_4OS$	386	2	4	3.8	5	96	4	557
Baricitinib	44205240	$C_{16}H_{17}N_7O_2S$	371	1	7	0.3	5	129	4	678
Binimetinib	10288191	$C_{17}H_{15}BrF_2N_4O_3$	441	3	7	2.6	6	88.4	3	521
Bosutinib	5328940	$C_{26}H_{29}Cl_2N_5O_3$	530	1	8	5.0	9	82.9	4	734
Brigatinib	68165256	$C_{29}H_{39}ClN_7O_2P$	584	2	9	5.2	8	85.9	5	835
Cabozantinib	25102847	$C_{28}H_{24}FN_3O_5$	501	2	7	4.5	8	98.8	4	795
Ceritinib	57379345	$C_{28}H_{36}ClN_5O_3S$	558	3	8	6.0	9	114	4	835
Cobimetinib	16222096	$C_{21}H_{21}F_3IN_3O_2$	531	3	7	5.1	4	64.6	4	624
Crizotinib	11626560	$C_{21}H_{22}Cl_2FN_5O$	450	2	6	4.4	5	78	4	558
Dabrafenib	44462760	$C_{23}H_{20}F_3N_5O_2S_2$	520	2	11	4.5	6	148	4	817
Dacomitinib	11511120	$C_{24}H_{25}ClFN_5O_2$	470	2	7	4.8	7	79.4	4	665
Dasatinib	3062316	$C_{22}H_{26}ClN_7O_2S$	488	3	9	3.0	7	135	4	642
Encorafenib	50922675	$C_{22}H_{27}ClFN_7O_4S$	540	3	10	3.1	10	149	3	836
Entrectinib	25141092	$C_{31}H_{34}F_2N_6O_2$	561	3	8	5.5	7	85.5	6	847
Erdafitinib	67462786	$C_{25}H_{30}N_6O_2$	446	1	7	4.6	9	77.3	4	583
Erlotinib	176870	$C_{22}H_{23}N_3O_4$	393	1	7	3.1	11	74.7	3	525
Everolimus	6442177	$C_{53}H_{83}NO_{14}$	958	3	14	4.5	9	205	3	1810
Fedratinib	16722836	$C_{27}H_{36}N_6O_3S$	525	3	9	4.9	11	117	4	787
Fostamatinib	11671467	$C_{23}H_{26}FN_6O_9P$	580	4	15	1.7	10	187	4	904
Gefitinib	123631	$C_{22}H_{24}ClFN_4O_3$	447	1	8	4.5	8	68.7	4	545
Gilteritinib	49803313	$C_{29}H_{44}N_8O_3$	552	3	10	3.0	9	121	5	785
Ibrutinib	24821094	$C_{25}H_{24}N_6O_2$	441	1	6	3.1	5	99.2	5	678
Imatinib	5291	$C_{29}H_{31}N_7O$	494	2	7	4.2	7	86.3	5	706
Lapatinib	208908	$C_{29}H_{26}ClN_4O_4S$	580	2	9	5.0	11	115	5	898
Larotrectinib	46188928	$C_{21}H_{22}F_2N_6O_2$	428	2	7	2.6	3	86	5	659
Lenvatinib	9823820	$C_{21}H_{19}ClN_4O_4$	427	3	5	3.6	6	116	4	634
Lorlatinib	71731823	$C_{21}H_{19}FN_6O_2$	406	1	7	2.0	0	110	3	700
Midostaurin	9829523	$C_{35}H_{30}N_4O_7$	571	1	4	5.3	3	77.7	5	1140
Neratinib	9915743	$C_{30}H_{29}ClN_6O_3$	557	2	8	5.1	11	112	4	881
Netarsudil	66599893	$C_{28}H_{27}N_3O_3$	454	2	5	4.2	8	94.3	4	678
Nilotinib	644241	$C_{28}H_{22}F_3N_7O$	530	2	9	5.0	6	97.6	5	817
Nintedanib	135423438	$C_{31}H_{33}N_5O_4$	540	2	7	3.9	8	102	5	947
Osimertinib	71496458	$C_{28}H_{33}N_7O_2$	500	2	7	3.4	10	87.6	4	752
Palbociclib	5330286	$C_{24}H_{29}N_7O_2$	448	2	8	0.3	5	103	5	775
Pazopanib	10113978	$C_{21}H_{23}N_7O_2S$	438	2	8	3.8	5	127	4	717
Pexidartinib	25151352	$C_{20}H_{15}ClF_3N_5$	418	2	7	4.5	5	66.5	4	537
Ponatinib	24826799	$C_{29}H_{27}F_3N_6O$	533	1	8	4.7	6	65.8	5	910
R406	11213558	$C_{22}H_{23}FN_6O_5$	470	3	11	3.1	7	129	4	691
Regorafenib	11167602	$C_{21}H_{15}ClF_4N_4O_3$	483	3	8	4.8	5	92.4	3	686
Ribociclib	44631912	$C_{23}H_{30}N_8O$	435	2	7	2.6	5	91.2	5	636
Ruxolitinib	25126798	$C_{17}N_{18}N_6$	306	1	4	2.0	4	83.2	4	453
Sirolimus	5284616	$C_{51}H_{79}NO_{13}$	914	3	13	4.5	6	195	3	1760
Sorafenib	216239	$C_{21}H_{16}ClF_3N_4O_3$	465	3	7	3.2	5	92.4	3	646
Sunitinib	5329102	$C_{22}H_{27}FN_4O_2$	398	3	4	3.2	7	77.2	3	636
Temsirolimus	6918289	$C_{56}H_{87}NO_{16}$	1029	4	16	4.3	11	242	3	2010
Tofacitinib	9926791	$C_{16}H_{20}N_6O$	312	1	5	1.0	3	88.9	3	488
Trametinib	11707110	$C_{26}H_{23}FlN_5O_4$	615	2	6	2.8	5	102	4	1090
Vandetanib	3081361	$C_{22}H_{24}BrFN_4O_2$	475	1	7	5.3	6	59.5	4	539
Vemurafenib	42611257	$C_{23}H_{18}ClF_2N_3O_3S$	490	2	7	4.9	7	100	4	790

[a] All data from NIH PubChem except for cLogP (the calculated Log_{10} of the partition coefficient, which was computed using MedChem Designer™, version 2.0, Simulationsplus, Inc. Lancaster, CA 93534).
[b] No. of hydrogen bond donors.
[c] No. of hydrogen bond acceptors.
[d] Calculated Log_{10} of the partition coefficient.
[e] (PSA) Polar surface area.
[f] Values obtained from https://pubchem.ncbi.nlm.nih.gov/.

N−H group of DFG-D796 (Fig. 5C). The therapeutic makes hydrophobic contact with five spine residues (RS2/3, CS6/7/8), two shell residues (Sh1/2), and the KLIFS-3 residue. It also makes hydrophobic contact with the β3-strand AVK616, I636 and M637 of the αC-helix, and DFG-D796. The trifluoromethyl group interacts with Trp550 within the juxtamembrane segment [73]. The drug occupies the front pocket, gate area, back pocket, BP-I-B, BP-II-out, and BP-V. The drug has the inactive DFG-D_{out} structure and the ligand extends past the gatekeeper leading to its classification of a type IIA inhibitor [23].

Fedratinib is an anilino-pyrimidine derivative that was approved in 2019 for the treatment of primary myelofibrosis and myelofibrosis secondary to polycythemia vera [74]. The hallmark of these maladies is the development of obliterative marrow fibrosis. There is extensive deposition of collagen in the marrow by non-neoplastic fibroblasts. The replacement of the bone marrow by fibrous tissue reduces bone marrow hematopoiesis and leads to extensive extramedullary hematopoiesis, principally in the spleen. The usual clinical manifestations of myelofibrosis include anemia, splenomegaly, bone pain, fatigue, and high uric acid levels that may lead to gout. A *JAK2 V617F* mutation occurs in about half of the patients with primary myelofibrosis. JAK2 contains a pseudokinase domain in the middle third and a functional kinase domain in the final third of the protein; the mutation occurs at the end of the β4-strand in the JAK2 pseudokinase domain [35]. The IC_{50} value of fedratinib for JAK2 is 6 nM; it also inhibits Flt3 and RET with IC_{50} values of 25 nM and 17 nM, respectively. Fedratinib decreased the spleen volume in 36–40 % of myelofibrosis patients [74]. Moreover, the majority of these patients with leukocytosis or thrombocytosis achieved normalization of these parameters after both six and twelve cycles of treatment [75].

Fedratinib also inhibits the action of bromodomain-containing proteins that function as transcriptional regulators, chromatin modulators, and chromatin modifying enzymes [76]. The bromodomain is a conserved 110-amino acid structural motif composed of four α-helices (αZ, αA, αB, and αC) that make up a left-handed bundle [77]. Two loop regions (ZA and BC) connect the α-helices and form a surface that interacts with acetylated lysine residues in nucleosomal histones. In humans, there are 61 bromodomains that occur within 42 multi-domain proteins that regulate transcription, including ATP-dependent chromatin remodeling complexes, transcriptional co-activators, histone acetyltransferases, and BET proteins (bromodomain followed by an extraterminal domain). Dysfunction of bromodomain-containing proteins is associated with the pathogenesis of various cancers [76,77]. Ciceri et al. hypothesize that single drugs that inhibit independent oncogenic pathways such as the JAK-STAT and bromodomain modules may improve the durability of clinical responses to targeted therapies [76]. However, what role, if any, that fedratinib inhibition of both (i) bromodomain-containing proteins and (ii) JAK2 plays in the clinical improvements observed in patients with myelofibrosis is unclear.

Unfortunately, there are no X-ray crystal structures of fedratinib (TG-101348) bound to JAK2 or any other protein kinase domain. However, the X-ray crystal structure of TG-101209 (a compound similar to fedratinib) bound to JAK2 has been reported (PDB ID: 4ji9) [78]. Fedratinib and TG-101209 are nearly identical except that fedratinib possesses an ethoxypyrrolidine side chain while TG-101209 has a methylpiperazine side chain. The X-ray crystal structure of TG-101209 bound to phosphorylated and activated JAK2 indicates that (i) the pyrimidine *N*1 forms a hydrogen bond with the N−H group of the third hinge residue and (ii) the 2-amino group N−H forms a hydrogen bond with the carbonyl group of the third hinge residue. The drug occurs in the front pocket of an active enzyme and is classified as a type I inhibitor. Whether fedratinib binds to JAK2 in a similar fashion remains to be determined.

After the approval of imatinib for the treatment of chronic myeloid leukemia in 2001, no small molecule protein kinase inhibitors were approved in 2002, 2003, 2008, 2010, and 2016. However, six new drugs were approved in 2012 and 2017 and nine drugs were approved in 2018 while a total of four small molecule protein kinase antagonists were approved in 2019. One can anticipate the approval of additional small molecule protein kinase inhibitors in the near future. However, these data demonstrate that the rate of year-to-year approval is sporadic.

6. Analyses of the physicochemical properties of orally effective drugs

6.1. Lipinski's rule of five (Ro5)

Pharmacologists and medicinal chemists have searched for advantageous drug-like chemical properties that result in pharmaceuticals with oral therapeutic effectiveness. Lipinski's "rule of five" is a computational and experimental technique that is used to estimate membrane permeability, solubility, and efficacy in the drug-development setting [55]. It is a rule of thumb that assesses drug-likeness and ascertains whether an entity with particular pharmacological activities has chemical and physical properties that suggest it would make an orally effective drug. The Lipinski criteria were based upon the finding that most orally effective therapeutics are comparatively small and moderately lipophilic molecules. The Ro5 criteria are used during drug development when pharmacologically active lead compounds are serially optimized to increase their selectivity and activity while maintaining their drug-like physicochemical properties.

The Ro5 predicts that less than ideal oral effectiveness is more likely to be observed when (i) the calculated Log P (cLogP) is greater than 5, when (ii) there are more than 5 hydrogen-bond donors, when (iii) there are more than 5 × 2 or 10 hydrogen-bond acceptors, and when (iv) the molecular weight is greater than 5 × 100 or 500 [55]. The partition coefficient (P) is the ratio of the solubility of the un-ionized compound in the organic phase of water-saturated n-octanol divided by its solubility in the aqueous phase. The P value is positively correlated with hydrophobicity; the larger the P value, the greater is the hydrophobicity. The number of hydrogen-bond donors is the sum of NH and OH groups and the number of hydrogen-bond acceptors consists of any heteroatom lacking a formal positive charge with the exception of heteroaromatic sulfur and oxygen atoms, pyrrole nitrogen atoms, halogen atoms, and higher oxidation states of sulfur, phosphorus, and nitrogen, but including the oxygen atoms bonded to them. Lipinski's Ro5 is based on the chemical properties of more than two thousand reference pharmaceuticals [55].

Excluding the macrolides, the average molecular weight (MW) of the small molecule FDA-approved protein kinase antagonists is 480 ranging from 306 (ruxolitinib) to 615 (trametinib) (Table 6). The compounds with a molecular weight greater than 500 include the three macrolides and fostamatinib (a prodrug that is converted to R406 with a molecular weight of 470), entrectinib, encorafenib, ceritinib, midostaurin, abemaciclib, bosutinib, brigatinib, cabozantinib, cobimetinib, nilotinib, dabrafenib, gilteritinib, ponatinib, lapatinib, neratinib, nintedanib, and trametinib. These findings demonstrate that there is a tendency for orally effective small molecule protein kinase pharmaceuticals to exceed the 500 Da molecular-weight criterion. Moreover, seven of the 52 approved drugs have a cLogP of greater than five; these include neratinib, abemaciclib, brigatinib, midostaurin, vandetanib, entrectinib, and ceritinib. Furthermore, dabrafenib, fostamatinib, and the three macrolides (sirolimus, everolimus, and temsirolimus) have more than ten hydrogen bond acceptors. Thus, a total of 22 of the 52 FDA-approved small molecule protein kinase therapeutics fail to conform to Lipinski's Ro5.

6.2. The importance of lipophilicity and ligand efficiency

6.2.1. Lipophilic efficiency, LipE

After the emergence of Lipinski's Ro5 in 2001 [55], later work on the physicochemical properties of orally effective therapeutics has led

to various refinements [79–86]. For example, lipophilic efficiency, or LipE, is a parameter that is exploited in drug discovery that combines potency and lipophilic-driven binding as a strategy to increase binding efficiency. Equations for calculating lipophilic efficiency are given by the following formulas:

$$\text{LipE} = \text{p}K_i - \text{cLogD} \text{ or } \text{LipE} = \text{p}IC_{50} - \text{cLogD}$$

Following its usage as expressing the molar hydrogen ion concentration as pH, the operator p represents the negative of the Log_{10} of the K_i or IC_{50}. Additionally, cLogD is the calculated Log_{10} of the Distribution coefficient; this represents the ratio of the drug solubility (both ionized and un-ionized) in the organic phase divided by its solubility in the aqueous phase of immiscible n-octanol/water at a specified pH, usually near 7.

The second term of the equation (– cLogD or minus cLogD) characterizes the lipophilicity of a pharmaceutical where c indicates that the value is calculated using an algorithm reliant upon the behavior of literally thousands of reference organic compounds. The greater the solubility of a compound in the organic phase of an immiscible n-octanol/water mixture, the greater is its lipophilicity, and the greater is the value of – cLogD. Leeson and Springthorpe hypothesize that drug lipophilicity, as assessed by its – cLogP value, is one of the more important characteristics that should be taken into account during drug development and discovery [81]. Their use of – cLogP was based upon experiments completed before the use of the distribution coefficient (D) became commonly available. For practical considerations, either cLog_{10}D or cLog_{10}P can be employed to compare a series of several compounds. A higher lipophilicity may play a substantial role in facilitating binding to adventitious targets leading to an increased number of adverse events. One objective for improving beneficial properties during drug development is to increase potency without concurrently increasing lipophilicity. Lipophilic efficiency aids in the optimization of lead compounds by enabling a direct evaluation of drug congeners; moreover, the same assay should be used in order to make the comparison of the drug congeners valid [84].

cLogD can be calculated for a series of compounds by computer in a matter of minutes. Because the investigational determination of Log_{10} of D is labor intensive, such experimental determinations are performed only in select cases. Optimal values of lipophilic efficiency values range from 5 to 10 [80]. Decreasing the lipophilicity and increasing potency during drug development and discovery generally produces therapeutics with better pharmaceutical properties. The average value of lipophilic efficiency for the FDA-approved small molecule protein kinase inhibitors is 4.92 with a range from 2 (vandetanib) to 8.5 (tofacitinib) (Table 7). More than half of the pharmaceuticals (29) have values that are less than 5 while the recommended optima range from 5 to 10.

6.2.2. Ligand efficiency, LE

The ligand efficiency (LE) is a property that relates the binding affinity, or potency, per non-hydrogen atom (heavy atom) of a drug. This value is calculated using the following formula:

$$\text{LE} = \Delta G^{\circ\prime\prime}/\text{N} = -\text{RT} \ln K_{eq}/\text{N} = -2.303\text{RT} \text{Log}_{10} K_{eq}/\text{N}$$

$\Delta G^{\circ\prime\prime}$ is the value of the standard free energy change of a compound binding to its enzyme target at neutral pH, N represents the number of heavy atoms (non-hydrogen atoms) in the drug, R represents the universal gas constant or energy-temperature coefficient, (0.00198 kcal/degree-mol), T signifies the absolute temperature in degrees Kelvin, and K_{eq} is the value of the equilibrium constant. Optimal values of ligand efficiency are greater than 0.3 kcal/mol [79,83]. The IC_{50} or K_i values are used for the equilibrium constant. At a physiological temperature of 37 °C (310 K), this equation becomes – (2.303 × (0.00198 kcal/mol-K) × 310 K Log_{10} K_{eq})/N or – 1.41 Log_{10} K_{eq}/N. Ligand efficiency was initially suggested as a methodology for comparing drug affinities based upon their average binding energy per atom. Moreover, ligand efficiency aids in the selection of lead compounds and is particularly useful

Table 7
Lipophilic efficiency (LipE) and ligand efficiency (LE) values and primary targets of FDA-approved drugs.

Drug	Target & kinase family[a]	K_i (nM)[b]	pK_i	cLogP[c]	LipE[d]	N[e]	LE[f]
Abemaciclib	CDK4, S/T	0.6	9.22	5.2	4.02	37	0.351
Acalbrutinib	BTK, NRY	3.1	8.51	1.1	7.41	35	0.343
Afatinib	EGFR, RY	0.5	9.33	4.0	5.33	34	0.387
Alectinib	ALK, RY	1.9	8.72	4.7	4.02	36	0.342
Axitinib	VEGFR2, RY	0.25	9.6	3.8	5.80	28	0.483
Baricitinib	JAK2, NRY	7	8.15	0.3	7.85	26	0.442
Binimetinib	MEK1, DS	12	7.92	2.6	5.3	27	0.414
Bosutinib	BCR-Abl, NRY	20	7.7	5.0	2.70	36	0.302
Brigatinib	ALK, RY	0.398	9.4	5.2	4.20	40	0.331
Cabozantinib	RET, RY	5	8.3	4.5	3.80	37	0.390
Ceritinib	ALK, RY	0.2	9.7	6.0	3.70	38	0.360
Cobimetinib	MEK1, DS	0.79	9.1	5.1	4.00	30	0.427
Crizotinib	ALK, RY	0.63	9.2	4.4	4.80	30	0.432
Dabrafenib	B-Raf, S/T	0.4	9.4	4.5	4.90	35	0.379
Dacomitinib	EGFR, RY	2.0	8.7	4.8	3.90	33	0.372
Dasatinib	BCR-Abl, NRY	0.16	9.8	3.0	6.80	33	0.419
Encorafenib	B-Raf, S/T	0.30	9.52	3.1	6.42	36	0.373
Erlotinib	EGFR, RY	0.32	9.5	3.1	6.40	29	0.462
Entrectinib	TRKA, RY	1	9.0	5.5	3.5	41	0.295
Erdafitinib	FGFR1, RY	2	8.7	4.6	4.1	33	0.372
Everolimus	FKBP12/mTOR, S/T	?	?	4.5	?	68	?
Fedratinib	JAK2, NRY	6	8.22	4.4	3.12	37	0.313
Fostamatinib	Syk, RY	17	7.77	1.7	6.07	40	0.274
Gefitinib	EGFR, RY	0.5	9.3	4.5	4.80	31	0.432
Gilteritinib	Flt3, RY	0.41	9.39	3.0	6.39	40	0.331
Ibrutinib	BTK, NRY	?	?	3.1	?	33	?
Imatinib	BCR-Abl, NRY	1	9.0	4.2	4.80	37	0.433
Lapatinib	EGFR, RY	1	9.0	5.0	4.00	40	0.325
Larotrectinib	TRK, RY	9.7	8.01	2.6	5.41	31	0.364
Lenvatinib	VEGFR2, RY	3.98	8.4	3.6	4.80	30	0.395
Lorlatinib	ALK, RY	9	8.05	2.0	6.05	30	0.378
Midostaurin	Flt3, RY	37	7.43	5.3	2.13	43	0.278
Neratinib	ErbB2/HER2, RY	59	7.23	5.1	2.13	40	0.255
Netarsudil	ROCK1/2, S/T	1	9	4.2	4.8	34	0.373
Nilotinib	BCR-Abl, NRY	12.5	7.9	5.0	2.90	39	0.286
Nintedanib	FGFR, RY	39.8	7.4	3.9	3.50	40	0.261
Osimertinib	EGFR, RY	7	8.15	3.4	4.75	37	0.311
Palbociclib	CDK4, S/T	10	8	0.3	7.70	33	0.342
Pazopanib	VEGFR2, RY	30	7.52	3.8	3.72	31	0.342
Pexidartinib	CSF1R, RY	13	7.89	4.5	3.4	29	0.384
Ponatinib	BCR-Abl, NRY	1	9	4.7	4.30	39	0.326
Regorafenib	VEGFR2, RY	4.2	8.4	4.8	3.6	33	0.359
Ribociclib	CDK4, S/T	10	8	2.6	5.40	32	0.353
Ruxolitinib	JAK1, NRY	1.2	8.92	2.0	7.92	23	0.608
Sirolimus	FKBP12/mTOR, S/T	?	?	4.5	?	65	?
Sorafenib	VEGFR1, RY	15.8	7.8	3.2	6.60	32	0.432
Sunitinib	VEGFR2, RY	3.98	8.4	3.2	5.20	29	0.408
Temsirolimus	FKBP12/mTOR, S/T	?	?	4.3	?	73	?
Tofacitinib	JAK1, NRY	0.79	9.1	1.0	8.50	23	0.582
Trametinib	MEK1, DS	3.4	8.47	2.8	6.00	37	0.345
Vandetanib	RET, RY	50	7.3	5.3	2.00	30	0.343
Vemurafenib	B-Raf, S/T	3.98	8.4	4.9	3.50	33	0.359

[a] NRY, non-receptor protein-tyrosine kinase; RY, receptor protein-tyrosine kinase; S/T, protein-serine/threonine kinase; DS; dual specificity protein kinase (catalyzes protein-tyrosine/threonine/serine phosphorylation but evolutionarily in the protein-serine/threonine kinase family).

[b] Representative values obtained from https://www.ebi.ac.uk/chembl/.

[c] Calculated value of the partition coefficient using MedChem Designer™ version 2.0 Simulationsplus, Inc. Lancaster CA 93534, USA.

[d] LipE = $p IC_{50}$ – cLogP, where cLogP is the calculated logarithm of the partition coefficient that was obtained using MedChem Designer™.

[e] N, Number of heavy atoms.

[f] LE = – 2.303 RT Log_{10} K_{eq}/N where N is the number of heavy (non-hydrogen) atoms in the drug.

in fragment-based drug discovery protocols [84].

Ligand efficiency corresponds to the binding affinity per heavy atom of the drug or ligand of interest. The value of N functions as a surrogate for the molecular weight. The equation that defines ligand efficiency indicates that the value is inversely proportional to the number of heavy atoms and is directly proportional to $-\ \mathrm{Log}_{10}\ K_{eq}$ (a positive number), or the binding affinity. The values of ligand efficiency based upon representative IC_{50} values for the FDA-approved small molecule protein kinase antagonists are provided in Table 7. With the exception of neratinib, nintedanib, fostamatinib, midostaurin, nilotinib, and entrectinib, the values fall within the optimal range and are greater than 0.3. The values for lipophilic efficiency (LipE) or ligand efficiency (LE) listed in Table 7 were calculated from data obtained under different experimental conditions. Accordingly, these values alone cannot be used to make a direct comparison of the drugs because different assay procedures were employed to obtain the data. However, these findings were derived from various drug discovery projects and are meant to provide a representative range of values. The primary kinase families that are inhibited by the FDA-approved drugs are also listed in Table 7.

6.2.3. Additional chemical descriptors of druglike properties

In an effort to improve oral effectiveness, not-unexpectedly, the Ro5 has generated many extensions and corollaries. For example, Veber et al. reported that the polar surface area (PSA) and the number of rotatable bonds has been found to differentiate between drugs that are orally active and those that are not for a large series of substances in rats [85]. These authors reported that ligands with polar surface area values less than or equal to 140 $Å^2$ demonstrate effective oral bioavailability. The polar surface area is taken as the sum of the surface over all polar atoms, primarily nitrogen and oxygen, but also including their linked hydrogen atoms. With the exception of dabrafenib, encorafenib, fostamatinib, and the macrolides, all of the FDA-approved small molecule protein kinase pharmaceuticals have a polar surface area less than 140 $Å^2$; the average value is 104 with a range from 59.5 (vandetanib) to 242 (temsirolimus) (Table 6). Moreover, these authors concluded that the optimal number of rotatable bonds should be less than or equal to 10. This descriptor is associated with molecular flexibility (degrees of freedom) and is considered to be an important influence in passive membrane permeation. Furthermore, the total number of degrees of freedom correlates with the entropy change of upon ligand binding and determines in part the binding affinity of drugs with their targets. With the exception of neratinib, erlotinib, lapatinib and temsirolimus, which have 11 rotatable bonds, all of the other drugs have 10 or fewer rotatable bonds. The average value is 6.6 and the number of rotatable bonds ranges from 0 (lorlatinib) to 11. Furthermore, Oprea found that the number of rings in most orally approved drugs is three or greater [86]. All of the approved small molecule protein kinase inhibitors have three or more rings with an average of 4.1, ranging from three to six. All of the FDA-approved drugs listed are orally effective with the exceptions of temsirolimus and netarsudil.

The molecular complexity of a drug is based upon the elements it contains, its structural features, and its symmetry. This parameter is computed using the Bertz/Hendrickson/Ihlenfelt algorithm [87,88]. It is based upon the number of atoms, their identity, the nature of the chemical bonds, and their bonding pattern. The molecular complexity ranges from 0 (simple ions) to several thousand (complex natural products). Intuitively, larger compounds usually possess a higher molecular complexity value than smaller ones. In contrast, molecules with few distinct atom types or elements and molecules that are highly symmetrical possess a lower molecular complexity value. All of the molecular complexity values for the FDA-approved drugs were obtained from PubChem (https://pubchem.ncbi.nlm.nih.gov/). For all of the FDA-approved drugs, the mean complexity value is about 800 with a range from 453 (ruxolitinib) to 2010 (temsirolimus). Not surprisingly, the large macrolide pharmaceuticals exhibit the greatest molecular complexity values. There are no recommended or optimal molecular complexity values for orally effective drugs; however, this property may be helpful as a parameter for determining the ease of drug synthesis, an important consideration in the commercial production of pharmaceutical agents.

7. Epilogue and perspective

Although great progress has been made in the development of small molecule protein kinase antagonists over the past 20 years, this field is still in its early stages. Most of the FDA- approved therapeutics are directed toward the treatment of various cancers and others are directed toward inflammatory diseases [9,89,90]. Entrectinib targets TRKA/B/C and ROS1 and was approved in 2019 for the treatment of solid tumors with NTRK fusion proteins and for ROS1-postive non-small cell lung cancer. Moreover, fedratinib blocks JAK2 and was approved for the treatment of myelofibrosis. Protein kinase inhibitors will undoubtedly be developed that target different protein kinases and more types of neoplasms. For example, pexidartinib is a CSF1R antagonist that was approved for the treatment of tenosynovial giant cell tumors and erdafitinib is a FGFR1/2/3/4 antagonist that was approved for the treatment of urothelial bladder cancers in 2019; CSF1R and FGFR1/2/3/4 are new targets and the giant cell tumors and urothelial bladder cancers represent new diseases that are being treated with small molecule protein kinase antagonists. Owing to the genomic instability of malignant cells, resistance to protein kinase therapeutics occurs on a regular basis. Such resistance has led to the development and discovery of second, third, and later generation medicinals that target the same enzyme and disease. Moreover, acquired drug resistance is frequently due to gatekeeper mutations in the target protein kinase [3]. For example, the T790 M mutation in *EGFR* is the third most frequently observed kinase mutation and it is responsible for about half of all instances of acquired EGFR inhibitor resistance. Although inflammatory processes are not characterized by genetic instability, it is currently unclear whether acquired resistance arises during in the treatment of inflammatory disorders.

Owing to the 244 protein kinases that map to cancer amplicons or disease loci [6], one can expect a substantial increase in the number of drugs inhibiting different protein kinases that will be used for the treatment of many more illnesses. The addition of new protein kinases to the therapeutic armamentarium will require the elucidation of the signaling pathways that participate in the pathogenesis of currently untargeted sicknesses. As the field matures during the next decades, one expects that protein kinase inhibitors with new scaffolds, chemotypes, and pharmacophores will be discovered. There are only two FDA-approved type III allosteric inhibitors (trametinib and cobimetinib) and these block the action of MEK1/2. One anticipates that additional allosteric inhibitors will be developed that target different enzymes in various signal transduction modules. Moreover, it is probable that new irreversible inhibitors that target protein kinases with –SH groups near the ATP-binding site will be forthcoming.

Although the development of protein kinase inhibitors represents a bona fide medical breakthrough, financial toxicity is one of the side effects associated with this class of drugs [91,92]. Moreover, the high cost of small molecule protein kinase inhibitors is one of the main drivers of increased financial toxicity [93]. The monthly expenditure per person taking these drugs in the United States ranges from $8,000–$20,000. Owing to cost-containment efforts, patients encounter higher co-payments for their pharmaceuticals and these co-payments may amount to 30 % of the price of the drug. One of the justifications that pharmaceutical companies provide for the rather high cost of these drugs is that considerable expenditures are required for their development. However, there is no evidence for an association between the costs of research, development, and clinical trials and drug prices [94]. Significantly, the rate of increase in drug prices in recent years has greatly exceeded that of the consumer price index. In reality, prescription drugs in the United States are priced on the basis of what the

market will bear.

The medical costs in ten high-income countries with publicly funded health care systems (Australia, Canada, Denmark, France, Germany, Japan, the Netherlands, Sweden, Switzerland, and the United Kingdom) were about one-half to two-thirds of those in the United States and the financial burden in other countries was considerably less than that in the US [95]. In 2016, the percentage of the gross domestic product spent on health care in the US was 17.8 % and spending in the ten other countries ranged from 9.6 % (Australia) to 12.4 % (Switzerland) with an overall average of 11.5 %. Administrative costs in the US accounted for 8 % compared with a range of 1–3 % in other countries as a percentage of overall health care expenditures. The earnings of physicians were also higher in the US. For example, the average salary for a general practitioner in the US was $218,000 and the overall mean salary of general practitioners reported in this study was $133,000. For pharmaceutical costs, spending per capita in the US was $1443 compared with a range of $466–$939 elsewhere. Owing to the intricacy of the commercially-driven health care system, it is unlikely that lower prices for drugs will occur in the United States in the near or distant future. Despite the greater expenditure for health care, the US ranked last in health care outcomes when compared with the ten high-income countries [95]. It had the lowest life expectancy, but the highest infant mortality, neonatal mortality, and maternal mortality rates.

Although employers in the United States pay an average of $28,000 annually for the health insurance for family of four, the required copayments contribute to the financial burden of cancer patients receiving protein kinase inhibitors, other targeted agents, and cytotoxic drugs. Consequently, patients often become noncompliant and take less than the prescribed amount of their medications or they forgo taking any at all [96,97]. Over a 13-year period (2000–2012), moreover, a total of 42 % of the 9.5 million newly diagnosed cancer patients in the United States lost all of their life savings within two years [98]. Not surprisingly, medical expenses are the most frequent cause of bankruptcy in the United States, accounting for 62 % of all personal bankruptcies. Unexpectedly, a total of 78 % of those who experienced medical bankruptcy had some form of health insurance. By including cost effectiveness in deciding which drugs to prescribe, clinicians have the ability to lower treatment costs, pressure pharmaceutical companies to constrain drug prices, and protect patients from financial toxicity. Prescribed medications represent the most common form of treatment in medical practice and they provide a major benefit for the health of individuals and nations, but unnecessarily high prices limit the ability of patients to benefit from these vital products. If people fail to take the prescribed therapeutic owing to the prohibitive cost, the development and discovery of these targeted protein kinase inhibitor treatments helps neither the patient nor the pharmaceutical company.

Declaration of Competing Interest

The author is unaware of any affiliations, memberships, or financial holdings that might be perceived as affecting the objectivity of this review.

Acknowledgment

The author thanks Laura M. Roskoski for providing editorial and bibliographic assistance. I also thank Jasper Martinsek and Josie Rudnicki for their help in preparing the figures and W.S. Sheppard and Pasha Brezina for their help in structural analyses. The colored figures in this paper were evaluated to ensure that their perception was accurately conveyed to colorblind readers [99].

Appendix A. Supplementary data

Supplementary material related to this article can be found, in the online version, at https://doi.org/10.1016/j.phrs.2019.104609.

References

[1] R. Roskoski Jr., A historical overview of protein kinases and their targeted small molecule inhibitors, Pharmacol. Res. 100 (2015) 1–23.
[2] P. Cohen, Protein kinases – the major drug targets of the twenty-first century? Nat. Rev. Drug Discov. 1 (2002) 309–315.
[3] G.K. Kanev, C. de Graaf, I.J.P. de Esch, R. Leurs, T. Würdinger, B.A. Westerman, et al., The landscape of atypical and eukaryotic protein kinases, Trends Pharmacol. Sci. 40 (2019) 818–832.
[4] F. Carles, S. Bourg, C. Meyer, P. Bonnet, PKIDB: a curated, annotated and updated database of protein kinase inhibitors in clinical trials, Molecules 23 (4) (2018), https://doi.org/10.3390/molecules23040908 pii: E908.
[5] P.M. Fischer, Approved and experimental small-molecule oncology kinase inhibitor drugs: a mid-2016 overview, Med. Res. Rev. 37 (2017) 314–367.
[6] G. Manning, D.B. Whyte, R. Martinez, T. Hunter, S. Sudarsanam, The protein kinase complement of the human genome, Science 298 (2002) 1912–1934.
[7] S.H. Myers, V.G. Brunton, A. Unciti-Broceta, AXL inhibitors in cancer: a medicinal chemistry perspective, J. Med. Chem. 59 (2016) 3593–3608.
[8] B.L. Roth, D.J. Sheffler, W.K. Kroeze, Magic shotguns versus magic bullets: selectively non-selective drugs for mood disorders and schizophrenia, Nat. Rev. Drug Discov. 3 (2004) 353–359.
[9] R. Roskoski Jr., Properties of FDA-approved small molecule protein kinase inhibitors, Pharmacol. Res. 144 (2019) 19–50.
[10] D.R. Knighton, J.H. Zheng, L.F. Ten Eyck, V.A. Ashford, N.H. Xuong, S.S. Taylor, et al., Crystal structure of the catalytic subunit of cyclic adenosine monophosphate-dependent protein kinase, Science 253 (1991) 407–414.
[11] D.R. Knighton, J.H. Zheng, L.F. Ten Eyck, N.H. Xuong, S.S. Taylor, J.M. Sowadski, Structure of a peptide inhibitor bound to the catalytic subunit of cyclic adenosine monophosphate-dependent protein kinase, Science 253 (1991) 414–420.
[12] S.S. Taylor, A.P. Kornev, Protein kinases: evolution of dynamic regulatory proteins, Trends Biochem. Sci. 36 (2011) 65–77.
[13] A.P. Kornev, S.S. Taylor, Dynamics-driven allostery in protein kinases, Trends Biochem. Sci. 40 (2015) 628–647.
[14] R. Roskoski Jr., Cyclin-dependent protein serine/threonine kinase inhibitors as anticancer drugs, Pharmacol. Res. 139 (2019) 471–488.
[15] S.K. Hanks, T. Hunter, Protein kinases 6. The eukaryotic protein kinase superfamily: kinase (catalytic) domain structure and classification, FASEB J. 9 (1995) 576–596.
[16] Madhusudan, E.A. Trafny, N.H. Xuong, J.A. Adams, L.F. Ten Eyck, S.S. Taylor, et al., cAMP-dependent protein kinase: crystallographic insights into substrate recognition and phosphotransfer, Protein Sci. 3 (1994) 176–187.
[17] J. Zhou, J.A. Adams, Participation of ADP dissociation in the rate-determining step in cAMP-dependent protein kinase, Biochemistry 36 (1997) 15733–15738.
[18] P.A. Schwartz, B.W. Murray, Protein kinase biochemistry and drug discovery, Bioorg. Chem. 39 (2011) 192–210.
[19] A.P. Kornev, S.S. Taylor, Defining the conserved internal architecture of a protein kinase, Biochim. Biophys. Acta 1804 (2010) 440–444.
[20] A.P. Kornev, N.M. Haste, S.S. Taylor, L.F. Eyck, Surface comparison of active and inactive protein kinases identifies a conserved activation mechanism, Proc. Natl. Acad. Sci. U. S. A. 103 (2006) 17783–17788.
[21] A.P. Kornev, S.S. Taylor, L.F. Ten Eyck, A helix scaffold for the assembly of active protein kinases, Proc. Natl. Acad. Sci. U. S. A. 105 (2008) 14377–14382.
[22] H.S. Meharena, P. Chang, M.M. Keshwani, K. Oruganty, A.K. Nene, N. Kannan, et al., Deciphering the structural basis of eukaryotic protein kinase regulation, PLoS Biol. 11 (2013) e1001690.
[23] R. Roskoski Jr., Classification of small molecule protein kinase inhibitors based upon the structures of their drug-enzyme complexes, Pharmacol. Res. 103 (2016) 26–48.
[24] R. Roskoski Jr., The ErbB/HER family of protein-tyrosine kinases and cancer, Pharmacol. Res. 79 (2014) 34–74.
[25] R. Roskoski Jr., ErbB/HER protein-tyrosine kinases: structures and small molecule inhibitors, Pharmacol. Res. 87 (2014) 42–59.
[26] R. Roskoski Jr., Small molecule inhibitors targeting the EGFR/ErbB family of protein-tyrosine kinases in human cancers, Pharmacol. Res. 139 (2019) 395–411.
[27] R. Roskoski Jr., The role of small molecule platelet-derived growth factor receptor (PDGFR) inhibitors in the treatment of neoplastic disorders, Pharmacol. Res. 129 (2018) 65–83.
[28] R. Roskoski Jr., Vascular endothelial growth factor (VEGF) and VEGF receptor inhibitors in the treatment of renal cell carcinomas, Pharmacol. Res. 120 (2017) 116–132.
[29] R. Roskoski Jr., The role of small molecule Kit protein-tyrosine kinase inhibitors in the treatment of neoplastic disorders, Pharmacol. Res. 133 (2018) 35–52.
[30] R. Roskoski Jr., ROS1 protein-tyrosine kinase inhibitors in the treatment of ROS1 fusion protein-driven non-small cell lung cancers, Pharmacol. Res. 121 (2017) 202–212.
[31] R. Roskoski Jr., A. Sadeghi-Nejad, Role of RET protein-tyrosine kinase inhibitors in the treatment RET-driven thyroid and lung cancers, Pharmacol. Res. 128 (2018) 1–17.
[32] R. Roskoski Jr., Anaplastic lymphoma kinase (ALK): structure, oncogenic activation, and pharmacological inhibition, Pharmacol. Res. 68 (2013) 68–94.
[33] R. Roskoski Jr., Anaplastic lymphoma kinase (ALK) inhibitors in the treatment of ALK-driven lung cancers, Pharmacol. Res. 117 (2017) 343–356.
[34] R. Roskoski Jr., The role of fibroblast growth factor receptor (FGFR) protein-tyrosine kinase inhibitors in the treatment of cancers including those of the urinary bladder, Pharmacol. Res. 151 (2020) 104567.
[35] R. Roskoski Jr., Janus kinase (JAK) inhibitors in the treatment of inflammatory and

neoplastic diseases, Pharmacol. Res. 111 (2016) 784–803.
[36] R. Roskoski Jr., Cyclin-dependent protein kinase inhibitors including palbociclib as anticancer drugs, Pharmacol. Res. 107 (2016) 249–275.
[37] R. Roskoski Jr., Targeting oncogenic Raf protein-serine/threonine kinases in human cancers, Pharmacol. Res. 135 (2018) 239–258.
[38] R. Roskoski Jr., ERK1/2 MAP kinases: structure, function, and regulation, Pharmacol. Res. 66 (2012) 105–143.
[39] R. Roskoski Jr., Targeting ERK1/2 protein-serine/threonine kinases in human cancers, Pharmacol. Res. 142 (2019) 151–168.
[40] R. Roskoski Jr., Allosteric MEK1/2 inhibitors including cobimetanib and trametinib in the treatment of cutaneous melanomas, Pharmacol. Res. 117 (2017) 20–31.
[41] R. Roskoski Jr., Src protein-tyrosine kinase structure, mechanism, and small molecule inhibitors, Pharmacol. Res. 94 (2015) 9–25.
[42] Y. Liu, K. Shah, F. Yang, L. Witucki, K.M. Shokat, A molecular gate which controls unnatural ATP analogue recognition by the tyrosine kinase v-Src, Bioorg. Med. Chem. 6 (1998) 1219–1226.
[43] A.C. Dar, K.M. Shokat, The evolution of protein kinase inhibitors from antagonists to agonists of cellular signaling, Annu. Rev. Biochem. 80 (2011) 769–795.
[44] P.M. Ung, R. Rahman, A. Schlessinger, Redefining the protein kinase conformational space with machine learning, Cell Chem. Biol. 25 (2018) 916-24.e2.
[45] F. Zuccotto, E. Ardini, E. Casale, M. Angiolini, Through the "gatekeeper door": exploiting the active kinase conformation, J. Med. Chem. 53 (2010) 2691–2694.
[46] L.K. Gavrin, E. Saiah, Approaches to discover non-ATP site inhibitors, Med. Chem. Res. 4 (2013) 41.
[47] V. Lamba, I. Ghosh, New directions in targeting protein kinases: focusing upon true allosteric and bivalent inhibitors, Curr. Pharm. Des. 18 (2012) 2936–2945.
[48] T.K. Johnson, M.B. Soellner, Bivalent inhibitors of c-Src tyrosine kinase that bind a regulatory domain, Bioconjug. Chem. 27 (2016) 1745–1749.
[49] R.A. Copeland, The drug-target residence time model: a 10-year retrospective, Nat. Rev. Drug Discov. 15 (2016) 87–95.
[50] O.P. van Linden, A.J. Kooistra, R. Leurs, I.J. de Esch, C. de Graaf, KLIFS: a knowledge-based structural database to navigate kinase-ligand interaction space, J. Med. Chem. 57 (2014) 249–277.
[51] J.J. Liao, Molecular recognition of protein kinase binding pockets for design of potent and selective kinase inhibitors, J. Med. Chem. 50 (2007) 409–424.
[52] A.J. Kooistra, A. Volkamer, Kinase-centric computational drug development, Ann Rep Med Chem 50 (2017) 197–236.
[53] D. Bajusz, G.G. Ferenczy, G.M. Keserá, Structure-based virtual screening approaches in kinase-directed drug discovery, Curr. Top. Med. Chem. 17 (2017) 2235–2259.
[54] P. Wu, T.E. Nielsen, M.H. Clausen, FDA-approved small-molecule kinase inhibitors, Trends Pharmacol. Sci. 36 (2015) 422–439.
[55] C.A. Lipinski, F. Lombardo, B.W. Dominy, P.J. Feeney, Experimental and computational approaches to estimate solubility and permeability in drug discovery and development settings, Adv. Drug Deliv. Rev. 46 (2001) 3–26.
[56] M. Menichincheri, E. Ardini, P. Magnaghi, N. Avanzi, P. Banfi, R. Bossi, et al., Discovery of entrectinib: a new 3-aminoindazole as a potent anaplastic lymphoma kinase (ALK), c-ros oncogene 1 kinase (ROS1), and pan-tropomyosin receptor kinases (pan-TRKs) inhibitor, J. Med. Chem. 59 (2016) 3392–3408.
[57] No authors listed. Entrectinib OK'd for cancers with *NTRK* fusions, NSCLC. Cancer Discov. 2019;9:OF2. doi: 10.1158/2159-8290.CD-NB2019-101.
[58] E. Cocco, M. Scaltriti, A. Drilon, NTRK fusion-positive cancers and TRK inhibitor therapy, Nat. Rev. Clin. Oncol. 15 (2018) 731–747.
[59] J.P. Solomon, I. Linkov, A. Rosado, K. Mullaney, E.Y. Rosen, D. Frosina, et al., NTRK fusion detection across multiple assays and 33,997 cases: diagnostic implications and pitfalls, Mod. Pathol. (2019), https://doi.org/10.1038/s41379–019–0324–7.
[60] Z.T. Al-Salama, S.J. Keam, Entrectinib: first global approval, Drugs 79 (2019) 1477–1483.
[61] L.J. Scott, Larotrectinib: first global approval, Drugs (2019), https://doi.org/10.1007/s40265-018-1044-x.
[62] A. Drilon, T.W. Laetsch, S. Kummar, S.G. DuBois, U.N. Lassen, G.D. Demetri, et al., Efficacy of larotrectinib in TRK fusion-positive cancers in adults and children, N. Engl. J. Med. 378 (2018) 731–739.
[63] Y. Loriot, A. Necchi, S.H. Park, J. Garcia-Donas, R. Huddart, E. Burgess, et al., Erdafitinib in locally advanced or metastatic urothelial carcinoma, N. Engl. J. Med. 381 (2019) 338–348.
[64] K.S. Hanna, Erdafitinib to treat urothelial carcinoma, Drugs Today 55 (2019) 495–501.
[65] H. Patani, T.D. Bunney, N. Thiyagarajan, R.A. Norman, D. Ogg, J. Breed, et al., Landscape of activating cancer mutations in FGFR kinases and their differential responses to inhibitors in clinical use, Oncotarget 7 (2016) 24252–24268.
[66] R. Dienstmann, J. Rodon, A. Prat, J. Perez-Garcia, B. Adamo, E. Felip, et al., Genomic aberrations in the FGFR pathway: opportunities for targeted therapies in solid tumors, Ann. Oncol. 25 (2014) 552–563.
[67] J. Gattineni, P. Alphonse, Q. Zhang, N. Mathews, C.M. Bates, M. Baum, Regulation of renal phosphate transport by FGF23 is mediated by FGFR1 and FGFR4, Am. J. Physiol. Renal Physiol. 306 (2014) F351–8.
[68] R.D. Kim, D. Sarker, T. Meyer, T. Yau, T. Macarulla, J.W. Park, et al., First-in-human phase I study of fisogatinib (BLU-554) validates aberrant fibroblast growth factor 19 signaling as a driver event in hepatocellular carcinoma, Cancer Discov. (2019) pii: CD-19-0555.
[69] X. Han, J. Yang, L. Li, J. Huang, G. King, L.D. Quarles, Conditional deletion of Fgfr1 in the proximal and distal tubule identifies distinct roles in phosphate and calcium transport, PLoS One 11 (2) (2016) e0147845.
[70] F. Facchinetti, A. Hollebecque, R. Bahleda, Y. Loriot, K.A. Olaussen, C. Massard, et al., Facts and new hopes on selective FGFR inhibitors in solid tumors, Clin. Cancer Res. (2019), https://doi.org/10.1158/1078-0432.CCR-19-2035 pii: clincanres.2035.2019.
[71] Y.N. Lamb, Pexidartinib: first approval, Drugs (2019), https://doi.org/10.1007/s40265-019-01210-0.
[72] W.D. Tap, H. Gelderblom, E. Palmerini, J. Desai, S. Bauer, J.Y. Blay, et al., Pexidartinib versus placebo for advanced tenosynovial giant cell tumour (ENLIVEN): a randomised phase 3 trial, Lancet 394 (2019) 478–487.
[73] W.D. Tap, Z.A. Wainberg, S.P. Anthony, P.N. Ibrahim, C. Zhang, J.H. Healey, et al., Structure-guided blockade of CSF1R kinase in tenosynovial giant-cell tumor, N. Engl. J. Med. 373 (2015) 428–437.
[74] H.A. Blair, Fedratinib: first approval, Drugs 79 (2019) 1719–1725.
[75] A. Pardanani, J.R. Gotlib, C. Jamieson, J.E. Cortes, M. Talpaz, R.M. Stone, et al., Safety and efficacy of TG101348, a selective JAK2 inhibitor, in myelofibrosis, J. Clin. Oncol. 29 (2011) 789–796.
[76] P. Ciceri, S. Müller, A. O'Mahony, O. Fedorov, P. Filippakopoulos, J.P. Hunt, et al., Dual kinase-bromodomain inhibitors for rationally designed polypharmacology, Nat. Chem. Biol. 10 (2014) 305–312.
[77] J.M. Sahni, R.A. Keri, Targeting bromodomain and extraterminal proteins in breast cancer, Pharmacol. Res. 129 (2018) 156–176.
[78] M. Siu, R. Pastor, W. Liu, K. Barrett, M. Berry, W.S. Blair, et al., 2-Amino-[1,2,4]triazolo[1,5-*a*]pyridines as JAK2 inhibitors, Bioorg. Med. Chem. Lett. 23 (2013) 5014–5021.
[79] A.L. Hopkins, C.R. Groom, A. Alex, Ligand efficiency: a useful metric for lead selection, Drug Discov. Today 9 (2004) 430–431.
[80] G.F. Smith, Medicinal chemistry by the numbers: the physicochemistry, thermodynamics and kinetics of modern drug design, Prog. Med. Chem. 48 (2009) 1–29.
[81] P.D. Leeson, B. Springthorpe, The influence of drug-like concepts on decision-making in medicinal chemistry, Nat. Rev. Drug Discov. 6 (2007) 881–890.
[82] S. Ekins, N.K. Litterman, C.A. Lipinski, B.A. Bunin, Thermodynamic proxies to compensate for biases in drug discovery methods, Pharm. Res. 33 (2016) 194–205.
[83] A.L. Hopkins, G.M. Keserü, P.D. Leeson, D.C. Rees, C.H. Reynolds, The role of ligand efficiency metrics in drug discovery, Nat. Rev. Drug Discov. 13 (2014) 105–121.
[84] P.D. Leeson, Molecular inflation, attrition, and the rule of five, Adv. Drug Deliv. Rev. 101 (2016) 22–33.
[85] D.F. Veber, S.R. Johnson, H.Y. Cheng, B.R. Smith, K.W. Ward, K.D. Kopple, Molecular properties that influence the oral bioavailability of drug candidates, J. Med. Chem. 45 (2002) 2615–2623.
[86] T.I. Oprea, Property distribution of drug-related chemical databases, J. Comput. Aided Mol. Des. 14 (2000) 251–264.
[87] S.H. Bertz, The first general index of molecular complexity, J. Am. Chem. Soc. 1103 (1981) 3559–3601.
[88] J.B. Hendrickson, P. Huang, A.G. Toczko, Molecular complexity: a simplified formula adapted to individual atoms, J Chem Inf Compout Sci 27 (1987) 63–67.
[89] K. Bechman, M. Yates, J.B. Galloway, The new entries in the therapeutic armamentarium: the small molecule JAK inhibitors, Pharmacol. Res. 147 (2019) 104392.
[90] K. Bechman, G.B. Galloway, K.L. Winthrop, Small-molecule protein kinase inhibitors and the risk of fungal infections. Curr. Fungal Infect. Rep. https://doi.org/10.1007/s12281-019-00350-w.
[91] H.M. Kantarjian, T. Fojo, M. Mathisen, L.A. Zwelling, Cancer drugs in the United States: *justum pretium*–the just price, J. Clin. Oncol. 31 (2013) 3600–3604.
[92] K.S.M. Smalley, Pharmacological research and cancer: a call to arms, Pharmacol. Res. 146 (2019) 104291.
[93] T. Yezefski, A. Schwemm, M. Lentz, K. Hone, V. Shankaran, Patient assistance programs: a valuable, yet imperfect, way to ease the financial toxicity of cancer care, Semin. Hematol. 55 (2018) 185–188.
[94] A.S. Kesselheim, J. Avorn, A. Sarpatwari, The high cost of prescription drugs in the United States: origins and prospects for reform, JAMA 316 (2016) 858–871.
[95] I. Papanicolas, L.R. Woskie, A.K. Jha, Health care spending in the United States and other high-income countries, JAMA 319 (2018) 1024–1039.
[96] S.Y. Zafar, J.M. Peppercorn, D. Schrag, D.H. Taylor, A.M. Goetzinger, X. Zhong, et al., The financial toxicity of cancer treatment: a pilot study assessing out-of-pocket expenses and the insured cancer patient's experience, Oncologist 18 (2013) 381–390.
[97] S.B. Dusetzina, A.N. Winn, G.A. Abel, H.A. Huskamp, N.L. Keating, Cost sharing and adherence to tyrosine kinase inhibitors for patients with chronic myeloid leukemia, J. Clin. Oncol. 32 (2014) 306–311.
[98] A.M. Gilligan, D.S. Alberts, D.J. Roe, G.H. Skrepnek, Death or debt? National estimates of financial toxicity in persons with newly-diagnosed cancer, Am. J. Med. 131 (2018) 1187–1199.
[99] R. Roskoski Jr., Guidelines for preparing color figures for everyone including the colorblind, Pharmacol. Res. 119 (2017) 240–241 Erratum in: Pharmacol Res 2019;139:569.